Running Title: CALCITE & DOLOMITE DIAGENESIS IN BAKKEN SANDS USING SIMS O ISOTOPE MICROANALYSIS

OXYGEN ISOTOPE MICROANALYSIS BY SECONDARY ION MASS SPECTROMETRY SUGGESTS CONTINUOUS 300-MILLION-YEAR HISTORY OF CALCITE CEMENTATION AND DOLOMITIZATION IN THE DEVONIAN BAKKEN FORMATION

MARK W. BRODIE[1], ANDREW C. APLIN[1], BRUCE HART[2], IAN J. ORLAND[3], JOHN W. VALLEY[3], ADRIAN J. BOYCE[4]

[1]Department of Earth Sciences, Durham University, Durham, DH1 3LE, UK

[2]Statoil Gulf Services LLC, 6300 Bridge Point Parkway, Austin, TX, 78730, USA

[3]WiscSIMS, Department of Geoscience, University of Wisconsin-Madison, Madison, Wisconsin 53706, USA

[4]Scottish Universities Environmental Research Centre, Rankine Avenue, East Kilbride, G75 0QF, UK

Corresponding author: a.c.aplin@durham.ac.uk

Keywords: Diagenesis, Calcite, Dolomitization, SIMS, Oxygen Isotopes

ABSTRACT

Calcite cementation and dolomitization are key diagenetic processes in many sedimentary systems. Unravelling detailed histories and timescales of cementation and replacement is, however, often compromised by the limited spatial resolution of many analytical techniques; in some cases multiple grains are co-analyzed so that diagenetic histories are blurred and reaction periods are difficult to establish. In this study we have used 10-micrometer-resolution, *in situ* secondary ion mass spectrometry to determine the oxygen isotope composition of 197 individual, 10-50-micrometer-size crystals of dolomite and calcite from six samples in a single core of Upper Devonian Middle Bakken Member siltstones and sandstones, the major tight oil formation of the Williston Basin, USA. This amount of data places important constraints on the range of temperatures and times that carbonate cementation and replacement occurred. Petrographic data show that microcrystalline calcite cement is an early phase, and combined with mineralogical data suggest that much of the dolomite replaces calcite. Over spatial scales of less than a centimeter, analyses of individual calcite crystals have a range of 5‰ for $\delta^{18}O$ in the group of crystals, and for the group of individual dolomite crystals, 10‰. These sub-centimeter ranges are as great as those observed in previous studies of carbonate cements sampled over many meters and remind us that previous low-resolution studies may have inadvertently analyzed mixed phases. There is no relationship between dolomite texture and isotopic composition at this spatial scale; microscale backscattered electron imagery and scanning electron microscopy cathodoluminescence zoning is seen, but cannot be resolved with a 10 micrometer spot size. Assuming, since it is an early cement, that calcite

precipitated from seawater ($\delta^{18}O$ = -1.5‰), it formed at *ca*. 15-40°C, mainly at the lower temperatures. Present-day formation waters in Devonian rocks in this region have oxygen isotope compositions of 7-8‰ VSMOW. Using these values as a likely dolomitizing fluid, we suggest that dolomitization occurred continuously between 40 and 140°C over 150 – 200 million years, most likely in a fluid with a high Mg/Ca ratio resulting from gypsum formation in local evaporites. We suggest that this exceptionally low rate of dolomitization was controlled by the low rate of supply of Mg in a very sluggish flow regime; dolomitization is incomplete because of a limited supply of Mg.

INTRODUCTION

Burial diagenesis transforms sediments into sedimentary rocks through a range of mechanical and chemical processes driven by changes in effective stress and the requirement that mineral assemblages attempt to achieve thermodynamic equilibrium as a function of temperature, pressure, and fluid composition (e.g., Bjørlykke 2014). Although the chemical diagenetic reactions are wide-ranging, depending for example on initial mineralogy and fluid chemistry, questions which are generic to all processes involve (a) the rate of reactions, (b) the extent to which a pre-defined "system" (for example a sand body) is chemically open or closed, and (c) whether or not the reactions occurred continuously or were punctuated (e.g., Giles 1997; Burley et al. 1989; Giles et al. 2000; Gluyas and Coleman 1992; Robinson and Gluyas 1992; Taylor et al. 2010; Bjørlykke and Jahren 2012; Bjørlykke 2014).

These fundamental questions continue to be asked, in part at least, because of limitations in the analytical techniques available to answer them. Many studies have used some combination of petrography, fluid inclusions, and stable isotopes to evaluate diagenetic histories (e.g. Haszeldine et al. 1984; Land et al. 1987; Glasmann et al. 1989; Brint et al. 1991; Aplin and Warren 1994; Williams et al. 1997; Sullivan et al. 1997; Taylor et al. 2000; Girard et al. 2001; Goldstein 2001; Marchand et al. 2002; Schmid et al. 2004). However, diagenetic silicate and carbonate minerals in sandstones commonly form grains or overgrowths on scales less than 100 micrometers and may have grown over many millions of years. Detailing growth histories of individual phases thus requires probes which can operate on a sub-10-micrometer scale. Conventional stable-isotope and fluid-inclusion studies cannot unravel these histories because (a) the resolution of isotopic analyses is

76 insufficient and (b) fluid inclusions tend to occur in specific locations of diagenetic phases,
77 for example at grain-overgrowth boundaries or in healed microfractures (e.g., Osborne and
78 Haszeldine 1993).

79 Oxygen isotopes preserve important information about the temperature at which minerals
80 form and the nature of the fluids from which they precipitate. Earlier isotopic studies on
81 diagenetic quartz and carbonate were made on whole overgrowths or areas sampled with
82 microdrills, and could not generate temporal data (Lee and Savin 1985; Land et al. 1987;
83 Brint et al. 1991; Hart et al. 1992; Macaulay et al. 1993; Aplin and Warren 1994; Taylor et al.
84 2000; McBride and Milliken 2006). *In situ* isotope studies on well-identified minerals can
85 overcome uncertainties of what is being analyzed, but neither the resolution (20–30 μm)
86 nor the precision (± 2‰; 2SD) of earlier work using single-collector secondary ion mass
87 spectrometers (SIMS) were sufficient to constrain growth histories (Graham et al. 1996;
88 Williams et al. 1997; Lyon et al. 2000; Girard et al. 2001; Marchand et al. 2002). Technical
89 advances in SIMS now allow *in situ* analyses to be made on 2-10-μm-diameter regions and
90 have revealed up to 10‰ ranges in $\delta^{18}O$ in single quartz overgrowths and carbonate
91 cements (Pollington et al. 2011; Harwood et al. 2013; Śliwiński et al. 2016b).

92 Carbonates are common and often pervasive cements in marine sandstones (e.g. Bjørkum
93 and Walderhaug 1990, 1993; Macaulay et al. 1993; Klein et al. 1999; Taylor et al. 2000;
94 McBride and Milliken 2006). Although significant carbonate cement can be formed during
95 early burial (e.g., Bjørkum and Walderhaug 1990; 1993), oxygen and carbon isotope data
96 often show a wide range of values which imply a range of precipitation temperatures and/or
97 fluid compositions (e.g., Klein et al. 1999; Taylor et al. 2000). However, detailed
98 petrography, for example using backscattered electron microscopy, commonly reveals

chemically distinct carbonate phases on a sub-millimeter scale (e.g., Hart et al. 1992; Taylor et al. 2000; Śliwiński et al. 2016b). This means that conventional isotope analyses, in which areas of at least a few millimeters are sampled, are likely to result in the analysis of mixed phases or of a single phase that has grown over a long period of time. Equally, studies which have used selective leaching to isolate compositionally distinct carbonate phases rely on the specificity of the leaching method (e.g., Macaulay et al. 1993; Klein et al. 1999). The nature of these analytical tools means that diagenetic histories are inevitably blurred or uncertain.

Dolomite and calcite grains examined in this study of the Upper Devonian Middle Bakken Member in North Dakota are often smaller than 100 micrometers. The use of high-resolution SIMS, an analytical tool which allows oxygen isotope data to be collected from areas 10 micrometers in diameter, is thus essential if the timing and evolution of fluids responsible for the formation of these diagenetic phases are to be unravelled accurately. The Bakken Formation has recently received much attention as a highly significant unconventional hydrocarbon accumulation, and the occurrence of both calcite and dolomite is central to the quality of the petroleum reservoir (e.g., Li et al. 2015). Previous work on the oxygen-isotope composition of carbonates in the Bakken has been limited to studies of calcite in fracture fills (Pitman et al. 2001), the bulk analysis of mixed carbonates (Karasinski 2006), and one grain-scale study (Staruiala et al. 2013). Here, we report oxygen isotope data obtained by SIMS on calcite and dolomite grains and focus on four questions: (a) over what temperature and period of time did the carbonate phases form; (b) was carbonate diagenesis continuous or punctuated; (c) is the dolomite a primary cement or did it form through dolomitization of earlier calcite (e.g., Warren 2000; Machel 2004); and (d) to what extent did diagenesis occur in a closed or open geochemical system?

GEOLOGICAL CONTEXT

The Upper Devonian-Lower Mississippian Bakken Formation was deposited over wide areas of the intracratonic Williston basin, which covers 770,000 km^2 of Montana, North Dakota, and South Dakota in the USA and parts of Saskatchewan and Manitoba in Canada (Fig. 1). The basin is structurally simple with an almost complete stratigraphic section and only gentle, low-wavelength folding (Webster 1984; Meissner 1991). The burial history, based on a well which has a stratigraphy very similar to that of the core used in this study and in which the Bakken is buried to essentially the same depth, is one of continual subsidence from deposition to *ca*. 50 Ma, followed by modest uplift and renewed subsidence from 35 Ma to the present day (Kuhn et al. 2012) (Fig. 1C). The present-day temperature for the samples of this study is around 125 °C with a modelled maximum temperature between 150 and 160 °C.

The Bakken is divided into three stratigraphic members (Fig. 2). The Upper and Lower members are both organic-rich shales whilst the Middle Bakken Member, the subject of this study, comprises a variably but often highly carbonate-cemented series of very fine-grained sandstones and siltstones deposited over large areas of a shallow, epicontinental sea (Meissner 1978; Freisatz 1995; Egenhoff et al. 2011). At the depocenter of the Williston Basin the Middle Bakken reaches a maximum thickness of 46 m but varies in thickness across the basin (Pitman et al. 2001). Most current work suggests that the Middle Bakken was deposited in a variety of shallow-marine environments during a Late Devonian to Early Mississippian regression (e.g., Li et al., 2015). Whilst the sedimentology of the Middle Bakken has been extensively described (McCabe 1959; Meissner 1978; Webster 1984;

145 Holland et al. 1987; Smith and Bustin 1996; Pitman et al. 2001; Egenhoff et al. 2011;
146 Egenhoff 2017), diagenetic studies are more limited. Nevertheless, pervasive early calcite
147 cement has been recognized in several studies (Last and Edwards 1991; Pitman et al. 2001;
148 Ferdous 2001; Li et al. 2015), along with the interpretation of several phases of dolomite
149 (Ferdous 2001).

150

151 **EXPERIMENTAL METHODS**

152 *Samples*

153 Samples for this study come from a single core drilled in McKenzie County, North Dakota,
154 USA (Fig. 1B). The core was described using the five facies associations defined by Simenson
155 (2010) in a study of the Middle Bakken from the Parshall Field, Mountrail County, North
156 Dakota. A total of 32 core plugs were taken over the full thickness of the Middle Bakken
157 section; 6 of the 32 samples were selected for this study, including samples from each of the
158 five different facies.

159

160 *Petrography*

161 Thin sections were cut perpendicular to bedding from core plugs and carbonate textures
162 investigated using both transmitted-light and electron microscopy. Transmitted-light
163 microscopy was carried out using a Nikon Eclipse 50iPOL polarizing microscope. 300 points
164 per sample were counted using a Petroglight petrographic point counter. The thin sections
165 were then coated with a 30 nm layer of carbon before analysis by electron microscopy.

Electron microscopy was performed at Durham University's GJ Russell Electron Microscopy Facility on a Hitachi SU 70 FEG SEM in secondary (SE) and backscatter (BSE) and Cathodoluminescence (CL) modes. Images were acquired at 15 kV, 2-4 nA and a working distance of 15-16 mm.

Dolomite crystal textures were classified using the scheme described by Sibley and Gregg (1987). Whilst proposed principally for dolomite crystals in carbonate rocks, this scheme is also appropriate for low-temperature, mixed clastic-carbonate systems like the Bakken because it focuses on the grain-boundary and grain-size relationships of individual crystals, which can be used to infer the genetic origin of each dolomite crystal class.

Scanning Electron Microscopy - Cathodoluminescence (SEM-CL) images were acquired on carbon-coated thin sections and round resin plugs using the Hitachi SU 70 FEG SEM with a Gatan Mono-CL detector operated in panchromatic mode. Images were obtained at an accelerating voltage of 10 kV and a working distance of 17 mm. Spectral information was obtained over a wavelength search range of 505 - 800 nm and a dwell time of approximately 3,200 µs per pixel for an image resolution of 2250 x 2250. Intensity values were corrected using the system response curve.

Using SEM-WDS, the elemental compositions of 58 calcite crystals and 155 dolomite crystals with different textures in 13 samples were determined, including the six samples on which SIMS analyses were performed. Analyses were repeated three times per crystal, and the results for each crystal are reported as the mean of the three analyses.

188 *Mineralogy*

189 Bulk mineralogy was determined by KT Geoservices (Table 1). X-ray diffraction (XRD)
190 analysis was conducted using a Siemens D500 automated powder diffractometer equipped
191 with a copper X-ray source (40 kV, 30 mA) and a scintillation X-ray detector. Both bulk and
192 clay (< 4 μm) analyses were conducted. Quantitative data were obtained from the whole-
193 rock pattern using whole pattern fitting (WPF) and Rietveld refinement methods.

194

195 *Bulk C and O Isotope Analysis*

196 The carbon and oxygen stable-isotope composition of bulk calcite and dolomite were
197 analyzed at the Scottish Universities Environmental Research Centre (SUERC) on an
198 Analytical Precision AP2003 mass spectrometer equipped with a separate acid injector
199 system (Table 1). We attempted to separate calcite and dolomite through the preferential
200 dissolution of calcite by reaction with 105% H_3PO_4 under a helium atmosphere at 70 °C. As
201 shown later, our results in fact indicate that the fine-grained dolomite in these samples was
202 also substantially dissolved with this method. Measured O isotope ratios are reported as per
203 mil deviations relative to Vienna standard mean ocean water (VSMOW) and C isotopes
204 relative to Vienna PeeDee Belemnite (VPDB) using conventional delta (δ) notation. Mean
205 analytical reproducibility based on replicates of the SUERC laboratory standard MAB-2
206 (Carrara Marble) was around ± 0.2‰ for both carbon and oxygen. MAB-2 is an internal
207 SUERC laboratory standard extracted from the same Carrara Marble quarry as the IAEA-CO-
208 1 international standard. It is calibrated against IAEA-CO-1 and NBS-19 and has exactly the
209 same C and O isotope values as IAEA-CO-1 (-2.5‰ and 2.4‰ VPDB respectively).

210

211 *Secondary Ion Mass Spectrometry*

212 *In-situ*, sub-grain-scale oxygen stable-isotope data were obtained using secondary ion mass
213 spectrometry. Based on their mineralogy and petrographic characteristics, six
214 representative samples were selected, one from each facies. Soluble organic matter was
215 removed using a standard, 96 hour soxhlet extraction procedure using a mixture of
216 dichloromethane and methanol. The samples were then mounted in epoxy resin in 1-inch
217 round plugs. Several crystals (2 or 3) of calcite standard UWC-3 ($\delta^{18}O_{VSMOW}$ of UWC-3 is
218 12.49‰ ± 0.03‰ 1 SD, n = 9; Kozdon et al. 2009) were mounted at the center of each
219 sample. The sample was then polished sequentially with 6 μm, 3 μm, and 1 μm diamond
220 paste on a low-nap pad. The final polish was obtained using a 0.05 μm colloidal alumina
221 solution on a vibrating pad for 30-200 seconds. The polished sample plugs were then gently
222 cleaned with deionized water and ethanol, and dried in a vacuum oven for 5 hours at 40°C.
223 To prevent charging during analysis, samples were coated with 60 nm gold. The flatness
224 across the samples was measured using a white-light profilometer across both the polished
225 rock, the mounted and polished calcite standard, and enclosing epoxy. The maximum
226 topography recorded was 3 μm (sample) and 7 μm (sample and standard). Analysis spots
227 were not placed near localized areas with relief > 3 μm.

228 *In-situ* oxygen isotope data were acquired using a CAMECA IMS 1280 large-radius multi-
229 collector ion microprobe at the WiscSIMS Laboratory at the University of Wisconsin-
230 Madison (Kita et al. 2009; Valley and Kita 2009). A $^{133}Cs^{+}$ primary ion beam with a current of
231 1.4 nA was focused at the analytical surface, resulting in ellipsoidal pits ca. 10 μm x 13 μm in

size. The typical secondary $^{16}O^-$ ion intensity for the 300 analyses of this study was approximately 2.5 x 10^9 cps.

Both before and after every set of 8-17 sample analyses, a sample-mounted calcite standard (UWC-3) was measured four times. As for conventional analyses, stable-isotope ratios are reported using the standard delta notation relative to VSMOW ($\delta^{18}O$ ‰). The reproducibility of each set of unknown samples is reported as 2 SD of the bracketing standard analyses; the average 2 SD of bracketed analyses was 0.27‰ (refer also to the supplementary material). Detailed analytical protocols can be found in Kita et al. (2009).

Initial SEM-EDX observations indicated the presence of iron in some of the dolomite crystals. Śliwiński et al. (2016a) show that the extent of isotopic fractionation occurring during SIMS analysis of carbonates (matrix effect) is a function of the concentration of iron. Thus, instrument standards for the dolomite – ankerite series were analyzed during the same SIMS session to ensure the accuracy and precision of analyses for the full range of potential carbonate chemistries. In addition, the carbonate in each pit analysed by SIMS was identified in the SEM, and the iron composition of the crystal measured using SEM-WDS (adjacent to the pit), using an INCA Wave 700 spectrometer WDS detector attached to a Hitachi SU-70 FEG SEM. The SEM "spot size" (beam diameter) was between 1.7 and 5 nm with an interaction depth of up to 800 nm and width of around 3 μm. To ensure that the analyses were of specific crystals, only crystals with the shortest visible length of > 2 μm were analysed. Three sets of standards were used for SEM-WDS: (a) an elemental cobalt instrument standard was used at the start of every session; (b) at the start and end of each analytical session, the calcite standard UWC-3 (see Kozdon et al. 2009) which was mounted to the center of all of the analyzed samples was measured five times; (c) a series of

carbonate standards with known chemical compositions (calcite, ankerite, dolomite, and siderite) were analyzed to measure accuracy and precision (see Supplementary Material 2). Using the results of SEM-WDS analysis, we used the mass bias calibration method proposed by Śliwiński et al. (2016a) to correct SIMS $\delta^{18}O$ measurements for the presence of iron in the dolomite crystals (Supplementary Material). Only 8 analyses required correction for the presence of iron, since iron contents were generally less than the detection limit of 0.1 wt. % FeO. The residual of the dolomite-ankerite calibration curve, fitted through seven standard materials measured during the same SIMS session, was 0.25‰.

RESULTS

Sedimentology, Mineralogy and Petrography

The Middle Bakken is a sedimentologically heterogeneous fine sandstone - siltstone unit that is pervasively but variably cemented by both calcite and dolomite. Using the framework provided by Simonsen (2010) and the sedimentologic description of this core by Li et al. (2015), five facies (B, C, D1, D2, and E) were defined from the base (3206 m) to the top (3182 m) of the core, with a gradational facies between B and C. Facies B comprises strongly bioturbated, argillaceous, calcareous sandstones and siltstones; facies C consists of very fine-grained sandstones and siltstones showing both planar and undulose lamination, with some thin mud-rich horizons; facies D1 is a fine-grained sandstone with common soft-sediment deformation features; facies D2 consists of a light brown to light gray, parallel to undulating-laminated, low-angle cross-laminated sandstone; facies E comprises a dark gray

siltstone interbedded with a light gray, thinly parallel-laminated, very fine-grained sandstone.

Core photographs taken with both white and UV light (Fig. 3) suggest that in all facies, there are multiple 2-30 cm-thick zones of layered or nodular diagenetic carbonate where porosity has been infilled to the extent that they do not contain fluorescing oil (i.e., calcite cementation pre-dated oil migration; Li et al. 2015). Other areas, which do contain fluorescing oil, are more lightly and/or more variably carbonate-cemented. Based both on the XRD analysis of 13 samples and point counting of 15 samples, calcite (both primary, bioclastic calcite and diagenetic calcite) constitutes 3-56% of the rock volume and diagenetic dolomite between 5 and 41% (Table 1). Total carbonate content (calcite plus dolomite, including bioclastic calcite) varies between 32 and 72%. The average minus-cement porosity is 42% (range 36-46%), close to depositional porosity, and suggesting that cementation started close to the sediment-water interface. The inverse correlation between the amounts of calcite and dolomite ($r^2 = 0.62$) lends support to the idea that dolomite is replacing calcite rather than being a primary cement.

At the core scale, calcite- and dolomite-cemented regions are present in approximately 70% of the core. In thin section, diagenetic calcite and dolomite cement occurs as bands. These bands vary in thickness from a couple of millimeters up to the size of the full section. Whilst in most instances the millimeter-scale bands form sharp contacts parallel to bedding, in some cases there is no clear lithological control on the morphology of the contact or the spatial distribution within the section.

Diagenetic calcite is observed in two textural types. By far the most volumetrically important texture (Type 1) is pervasive, poikilotopic cement in which detrital grains “float”

299 within the calcite (Figs. 4D and 5A). Similar, early, massive calcite cement is common in
300 shallow-marine sandstones (e.g., Bjørkum and Walderhaug 1993). Type 2 calcite comprises
301 individual crystals which (a) appear to cement small numbers of grains to form a globular
302 morphology (Fig. 5B), and (b) occur as individual, discrete grains which do not connect other
303 grains; visual estimates from SEM show that these phases form < 1% of calcite.

304 Dolomite occurs as six different morphologies. Type 1 dolomites are nonplanar, anhedral,
305 crystals with rounded edges, 15-30 μm in size (Fig. 6A). Type 2 dolomites are euhedral
306 rhombs, 10-50 μm in size with micrometer-scale pores in their core (Fig. 6B). Type 3
307 dolomites are euhedral rhombs, 10-50 μm in size but without pores (Fig. 6C). Type 4
308 dolomites are subhedral, geometric, angular crystals which vary in size from 5 to 35 μm (Fig.
309 6D). Type 5 dolomites are 2-10-μm-thick ferroan rims which form around more
310 stoichiometric, iron-poor dolomite. This phase has been observed around all other dolomite
311 types (Fig. 6E). Type 6 dolomites are euhedral rhombs which are less than 5 μm in diameter
312 (Fig. 6F). Under transmitted light, some dolomites show a “cloudy core” texture which has
313 been previously suggested to result from the dolomitization of a calcite precursor, resulting
314 in a close-to-stoichiometric dolomitic outer zone and a more calcium-rich and porous core
315 (Murray and Lucia 1967; Sibley 1982).

316 In most cases, except in the relatively unusual cases of Fe enrichment towards the edge of
317 crystals, BSEM shows no evidence of significant changes in the chemical composition of
318 dolomite crystals from core to edge. Scanning electron microscopy - cathodoluminescence
319 (SEM-CL) does however reveal zoning within individual dolomite crystals. Zones of different
320 luminescence can reflect both subtle changes in crystal chemistry and/or variations in
321 growth mechanisms (e.g. Boggs and Krinsley 2006), and our data are insufficient to

322 determine the reasons for the zonation. In total, 48 crystals were viewed in 10 samples. The
323 CL character of individual dolomite types was consistent in all the samples and is reported in
324 Figure 7. All dolomite phases luminesce in the red part of the spectrum, including the "dull"
325 zones which simply have a lower - intensity luminescence (Fig. 7). Anhedral, Type 1
326 dolomites show incomplete concentric zones which have decreasing luminescence intensity
327 towards the edge of the crystals. Textural types 2-4 and 6 exhibit similar CL characteristics: a
328 single, concentric, low - intensity luminescence zone around a much more intensely
329 luminescing core. The rims are approximately 1-10 μm in thickness (Fig. 6E). Type 5
330 dolomites are ferroan rims which form single homogeneous layers around other dolomite
331 crystals; they show low emission intensity in the red spectrum.

332

333 *Chemical Composition*

334 Calcite cement has a very consistent chemistry, averaging 97.4 mol % Ca, 2.4 mol % Mg, and
335 0.2 mol % Fe (Fig. 8). Eighty percent of dolomite analyses have chemical compositions
336 between $Ca_{0.55}Mg_{0.45}CO_3$ and $Ca_{0.45}Mg_{0.55}CO_3$, with a modal value close to that of
337 stoichiometric dolomite. There is no obvious relation between dolomite composition and
338 textural type (Fig. 8). Almost all dolomites have low iron contents, with 85% containing less
339 than 2 mol % Fe and only 2 % with more than 6 mol % Fe. Note however that because of
340 their spatial scale, Type 5 dolomites (ferroan dolomite rims) were not systematically
341 measured, although they quite commonly form either as discrete rims or more diffuse
342 alteration zones around all other textural types of dolomite; they also form small, individual
343 crystals with anhedral to euhedral habits.

344 Diagenetic dolomite containing more than 55 mol % Mg are uncommon in the literature;
345 however, in this study, 17% of the analyses are more Mg-rich than $Ca_{0.45}Mg_{0.55}CO_3$. Most of
346 these analyses are from Samples 2 and 4, and the most common chemistry is around
347 $Ca_{0.4}Mg_{0.6}CO_3$, i.e., between the composition of stoichiometric dolomite ($Ca_{0.5}Mg_{0.5}CO_3$) and
348 huntite ($Ca_{0.25}Mg_{0.75}CO_3$).

349

350 *Bulk C and O Isotope Composition*

351 The results of bulk carbon and oxygen isotope analyses are reported in Table 1. The ranges
352 for putative calcite and dolomite overlap substantially and are approximately -3 to +3‰ for
353 carbon and +20 to +30 ‰ for oxygen (putative dolomite) and +22 to +26‰ (putative
354 calcite). We use "putative" because with the benefit of the SIMS oxygen isotope analyses of
355 individual calcite and dolomite crystals (see below) it is clear that the selective leach
356 partially dissolved dolomite as well as calcite. This is readily understood, as, in practice, the
357 "calcite" fraction is that gas extracted from the bulk samples after three hours of acid
358 digestion in a vacuum; the "dolomite" fraction is the gas then extracted after a further 24-
359 hour acid digestion on the residue (both corrected back to original carbonate as true calcite
360 or dolomite). Whilst such "dolomite" analyses are likely to be free of calcite, the "calcite" is
361 susceptible to contamination, as is shown by this study. Retrospectively, the advice is to
362 proceed with caution when interpreting previous studies, which have used similar selective
363 leaching techniques in an attempt to separate finely intergrown calcite and dolomite,
364 particularly with the "calcite" data.

365 The main result of the bulk isotope analyses is that most of the carbon in both dolomite and
366 (probably) calcite is from marine carbonate, with only minor inputs from organic sources.
367 Values between -3‰ and +3‰ suggest the addition of relatively small amounts of organic
368 carbon from processes involving coupled methanogenesis and CO_2 reduction, which would
369 result in more positive values, and from the oxidation of organic matter, which would result
370 in more negative values (e.g., Curtis et al. 1986).

371

372 *SIMS: Grain-Scale Oxygen Isotope Data*

373 Three hundred and eight sites were analyzed from the six samples selected for SIMS
374 analysis. After analysis, SEM was used to examine the shape of the pits formed by the ion
375 beam. Previous work (Cavosie et al. 2005; Linzmeier et al. 2016) has shown that data from
376 morphologically irregular pits are less reliable than those from regularly shaped pits. In this
377 study we took a very strict approach to ensure that only the most reliable data were
378 included. Some data were rejected due to the very fine nature of these samples, such that
379 some mixed phases were measured. Most of the rejected data are in fact from crystals with
380 minor irregularities such as surface asperities. All rejected data are reported in the
381 Supplementary Material. Using these strict criteria, we accepted 197 analyses, i.e., between
382 16 and 46 analyses from six sample areas, each of which is approximately 5 mm in diameter.

383 Values of $\delta^{18}O$ for individual calcite grains are almost all between +28.9 and + 33.7‰ (-1.9 –
384 2.8 ‰ VPDB), with a similar range in samples from each facies (Fig. 9). For dolomite, the full
385 range is +22.5 – 32.2‰ (-8.1 – 1.3 ‰ VPDB), with a mean value of +26.8‰ and with 93% of
386 values between +24 and +30‰ (Fig. 9). There is a similar range of $\delta^{18}O$ values in each

morphological type of dolomite. There is no relation between $\delta^{18}O$ and the Ca/Mg ratio of dolomite.

DISCUSSION

The oxygen isotope data in this study show as great a range on a sub-centimeter scale as many studies have found on conventional studies of diagenetic carbonates in sandstones sampled on scales of many meters (e.g., Bjørkum and Walderhaug 1993; Klein et al. 1999; Taylor et al. 2000). Given the sub-millimeter complexity observed in this study (Fig. 10), it is clear that conventional sampling methods can easily homogenize complex mixtures and result in an enforced, simplistic picture of diagenetic histories. Equally, however, our results show an overall commonality from sample to sample which show that carbonate diagenesis, although complex on a sample scale, proceeded in a similar way throughout fifteen meters of the Middle Bakken. With SIMS, the large number of analyses of accurately identified mineral phases allows us to draw a temporal picture of diagenesis which is not possible with conventional data. As we discuss below, our data suggest that carbonate diagenesis in the Middle Bakken was not episodic but occurred continuously over an approximately 300-million-year period of burial.

High minus-cement porosities suggest that diagenetic calcite started to precipitate close to the sediment-water interface, as observed in many similar studies (e.g., Wilkinson 1991; Gluyas and Coleman 1992; Bjørkum and Walderhaug 1990; 1993; Taylor et al. 2000). Our isotopic data support the early formation of calcite. Using the isotope paleothermometer proposed by O'Neil et al. (1969) for calcite and assuming a $\delta^{18}O$ of = -1.5‰ for Late

409 Devonian seawater (Hudson and Anderson 1989; van Geldern et al. 2006), the vast bulk of
410 calcite formed between 15 and 35 °C (Fig. 11).

411 The temperature histogram in Figure 11A suggests that the bulk of calcite cementation
412 occurred between 15 and 20 °C with steadily decreasing amounts at higher temperatures.
413 Assuming a mean seawater temperature of 15 °C, a geothermal gradient of 25 °C/km, and
414 an unchanging $\delta^{18}O_{H2O}$, calcite cementation occurred at decreasing rates during burial to *ca*.
415 800 meters. Linking this to the burial history (Fig. 1), calcite cementation occurred over the
416 first *ca*. 10 million years of burial. Given the occurrence of bioclasts in the Middle Bakken
417 and the carbon isotope signature of calcite (0 ± 3‰), this calcite most likely represents the
418 redistribution of biogenic calcite via local dissolution and precipitation.

419 Petrographic observations of (a) cloudy cores (transmitted light) and (b) porosity which
420 likely results from the volume reduction associated with the replacement of calcite by
421 dolomite (Weyl, 1960), combined with (c) the inverse correlation between the amounts of
422 dolomite and calcite, suggest that dolomite is largely replacing calcite rather than occurring
423 as a pore-filling cement. In the absence of reaction fronts in individual crystals, it appears
424 that dolomitization is a dissolution – precipitation reaction in which calcite is dissolved and 5
425 – 50-micrometer-size dolomite crystals are precipitated. The carbon isotope data for
426 dolomite and calcite-dolomite mixtures are similar and are thus also consistent with
427 dolomitization of calcite. Using the oxygen isotope paleothermometer proposed for
428 dolomite by Vasconcelos et al. (2005) for dolomite-water and assuming, as a first estimate,
429 that dolomite formed in unmodified seawater ($\delta^{18}O_{H2O}$= -1.5‰), a temperature range of 13
430 - 66°C is calculated (Fig. 11B). Based on a correlation between $\delta^{18}O$ and the Ca content of
431 diagenetic dolomites, Vahrenkamp et al. (1994) suggested that when estimating

precipitation temperatures for dolomite, a correction of +0.1 per mil may be needed per mol % of Mg deficiency due to variations in mineral-water isotope fractionation factors. For most of our data, this results in a correction of only < 0.3‰, with a maximum correction of 1.5‰; the range of estimated precipitation temperatures remains unchanged.

Since dolomite is supersaturated in seawater, dolomitization in unmodified seawater is geochemically feasible, but unusual (e.g., Machel 2004). Dolomitization more commonly occurs in fluids in which the Mg/Ca ratio has been modified as a result of evaporation and precipitation of gypsum (e.g., Budd 1997; Warren 2000; Machel 2004 for reviews). Anhydrite-bearing evaporites occur both below (Devonian Prairie Evaporite and Three Forks formations) and above (Mississippian Charles Salt Formation) the Bakken Formation, and pre-Mississippian waters in this part of the Williston Basin are commonly hypersaline and are likely dolomitizing fluids (Iampen and Rostron 2000). Values of $\delta^{18}O$ for present-day formation waters from the Devonian Duperow aquifer, which occurs below the Bakken in this part of the Williston Basin, are around +7.5 ‰ (Figure 1A; Rostron and Holmden 2003). If we assume a value of +7.5‰, the maximum calculated precipitation temperature is 157 °C, approximately that of the maximum burial temperature (Fig. 11D). If all dolomite formed from water with $\delta^{18}O$ = +7.5‰, then precipitation temperatures range from 61 to 157 °C (Fig. 11D). Slightly lower $\delta^{18}O$ values, for example +7‰, would give a temperature range of 58 – 150 °C. The histogram of estimated precipitation temperatures shows that the rate of dolomitization increases steadily from 60 to 130 °C and then decreases at higher temperatures (Figure 11D). Given that dolomitization rates increase with temperature, the limited reaction at the highest temperatures might reflect the generation of petroleum from the organic-rich shales above and below the middle Bakken and its emplacement into the

middle Bakken. If we assume that dolomitization occurred in fluids that evolved steadily from the original seawater (-1.5‰) to the present-day brine (+7.5‰), then dolomite would have formed throughout almost the whole burial history of the Bakken (Figs. 1, 11). In either case, dolomitization occurred continuously over approximately 150 – 250 million years.

The rate of dolomitization depends on a range of factors, including the Mg:Ca ratio in solution (Kaczmarek and Sibley 2007), the mineralogy of the reactant (Gaines 1974), and reactant surface area (Sibley et al. 1987). Rate constants for dolomite precipitation have been measured experimentally (Arvidson and Mackenzie 1999), and even at low diagenetic temperatures the resulting kinetics show that pervasive dolomitization and dolomite precipitation can occur on timescales of less than one million years (Whitaker and Xiao 2010; Al Helal et al. 2012); this is consistent with the occurrence of Holocene dolomites in modern sabkhas and carbonate islands (Budd 1997). Dolomitization rates increase markedly with increasing temperature (Arvidson and Mackenzie 1999) so that at the estimated temperatures of dolomitization in the Bakken (61 – 157 °C), rates are not controlled by kinetics. Rather, we suggest that the rate of dolomitization must be limited by the rate at which Mg is delivered to reaction sites and thus the fluid flow regime (Machel 2004; Whitaker et al. 2004). We have no way of evaluating the detailed flow history through the Bakken in North Dakota, but the highly saline and isotopically evolved waters which occur in the region today are likely to be part of an ancient, highly restricted and almost stagnant flow system (Rostron and Holmden 2003). With no topographic recharge in the area, fluid flow would be driven almost entirely by sediment compaction, with very low water:rock ratios. The lack of fluid flow and related supply of Mg is the most likely reason why

477 dolomitization, despite the length of time available for reaction, is partial rather than
478 complete.

479 As in almost all diagenetic studies, the lack of constraint of paleo-$\delta^{18}O_{H2O}$ limits our ability to
480 generate highly constrained diagenetic time-temperature histories. In principle, clumped-
481 isotope studies will allow this because precipitation temperatures can be fixed without the
482 need to assume $\delta^{18}O_{H2O}$ (Dale et al. 2014; Millán et al. 2016). However, the sample sizes
483 currently required for clumped-isotope work precludes the grain-scale analyses such as
484 those reported here. For the finely intergrown dolomites and calcites analyzed in this study,
485 clumped isotopes would have yielded a range of temperatures depending on the mixture of
486 calcite and dolomite grains drilled from each sample.

487

488 **SUMMARY AND CONCLUSIONS**

489 Shallow-marine fine-grained sandstones and siltstones from the Devonian Middle Bakken
490 Member are pervasively cemented with calcite and dolomite. Petrographic and
491 mineralogical data show that dolomite occurs as a result of dolomitization of calcite.

492 The oxygen isotope composition of 57 individual calcite and 174 individual dolomite grains
493 from six samples were determined using SIMS. A similarly wide range of values occurs in all
494 six samples: 5‰ for calcite and 10‰ for dolomite. For dolomite, there is no relationship
495 between morphology, chemistry, and isotopic composition, so that in this case petrography
496 is not a good guide to diagenetic history.

Since all samples display the same range of oxygen isotope values, we conclude that whilst carbonate diagenesis in the Middle Bakken is heterogeneous on a millimetre scale, the same set of diagenetic processes are occurring on the same timescales on a 20-meter scale. Furthermore, the range of oxygen isotope compositions that occur on a millimeter scale are similar to the total ranges determined in many conventional isotope studies of carbonate-cemented sandstones sampled on scales greater than a meter. It is likely that either mixed phases or isotopically diverse single phases have been analyzed in previous studies, resulting in blurred or incorrect diagenetic histories.

A great benefit of SIMS is that through the generation of a large number of analyses of known phases, a much more accurate diagenetic history can be elucidated compared to conventional studies in which either sample numbers are restricted or there is uncertainty over what phases have been analyzed. In this study we can be confident that carbonate diagenesis has been almost continuous from deposition to maximum burial: a period of 300 million years. Within the uncertainty of $\delta^{18}O_{H2O}$, calcite formed over the first *ca*. 10 Myr of burial, with most forming close to the sediment water interface. Dolomitization occurred continuously from *ca*. 61 – 157 °C over 150 – 250 million years. The rate of dolomitization was probably controlled by the rate of supply of Mg in a very sluggish flow regime; dolomitization is probably incomplete because of a lack of Mg and perhaps, in this case, by the fact that petroleum was emplaced into the sandstone late in the burial history.

REFERENCES

518 Al-Helal, A.B., Whitaker, F.F., and Xiao, Y., 2012, Reactive transport modeling of brine reflux:
519 dolomitization, anhydrite precipitation, and porosity evolution: Journal of Sedimentary
520 Research, v. 82, p. 196-215.

521

522 Aplin, A.C., and Warren, E.A., 1994, Oxygen isotopic indications of the mechanisms of silica
523 transport and quartz cementation in deeply buried sandstones: Geology, v. 22, p. 847-850.

524

525 Arvidson, R.S., and Mackenzie, F.T., 1999, The dolomite problem: control of precipitation
526 kinetics by temperature and saturation state: American Journal of Science, v. 299, p. 257-
527 288.

528

529 Bjørkum, P.A., and Walderhaug, O., 1990, Geometrical arrangement of calcite cementation
530 within shallow marine sandstones: Earth-Science Reviews, v. 29, p. 145-161.

531

532 Bjørkum, P.A., and Walderhaug, O., 1993, Isotopic composition of a calcite-cemented layer in
533 the Lower Jurassic Bridport Sands, southern England: implications for formation of laterally
534 extensive calcite-cemented layers: Journal of Sedimentary Research, v. 63, p. 678-682.

535

536 Bjørlykke, K., 2014, Relationships between depositional environments, burial history and
537 rock properties: Some principal aspects of diagenetic process in sedimentary
538 basins. Sedimentary Geology, v. 301, p. 1-14.

539

540 Bjørlykke, K., and Jahren, J., 2012, Open or closed geochemical systems during diagenesis in
541 sedimentary basins: Constraints on mass transfer during diagenesis and the prediction of
542 porosity in sandstone and carbonate reservoirs: American Association of Petroleum
543 Geologists, Bulletin, v. 96, p. 2193-2214.

544

545 Boggs, S., and Krinsley, D., 2006, Application of Cathodoluminescence Imaging to the Study of
546 Sedimentary Rocks: Cambridge, UK, Cambridge University Press, 146 p..

547

548 Brint, J.F., Hamilton, P.J., Haszeldine, R.S., Fallick, A.E., and Brown, S., 1991, Oxygen isotopic
549 analysis of diagenetic quartz overgrowths from the Brent sands: a comparison of two
550 preparation methods: Journal of Sedimentary Research, v. 61, p. 527-533.

551

552 Budd, D.A., 1997, Cenozoic dolomites of carbonate islands: their attributes and origin: Earth-Science
553 Reviews, v. 42, p. 1-47.

554

555 Burley, S.D., Mullis, J.T., and Matter, A., 1989, Timing diagenesis in the Tartan Reservoir (UK
556 North Sea): constraints from combined cathodoluminescence microscopy and fluid inclusion
557 studies: Marine and Petroleum Geology, v. 6, p. 98-120.

558

559 Cavosie, A.J., Valley, J.W., and Wilde, S.A., 2005, Magmatic $\delta^{18}O$ in 4400–3900 Ma detrital
560 zircons: a record of the alteration and recycling of crust in the Early Archean: Earth and
561 Planetary Science Letters, v. 235, p. 663-681.

562

563 Curtis, C.D., Coleman, M.L., and Love, L.G., 1986, Pore water evolution during sediment
564 burial from isotopic and mineral chemistry of calcite, dolomite and siderite
565 concretions: Geochimica et Cosmochimica Acta, v. 50, p. 2321-2334.

566

567 Dale, A., John, C.M., Mozley, P.S., Smalley, P.C., and Muggeridge, A.H., 2014, Time-capsule
568 concretions: unlocking burial diagenetic processes in the Mancos Shale using carbonate
569 clumped isotopes: Earth and Planetary Science Letters, v. 394, p. 30-37.

570

571 Egenhoff, S.O., 2017, The lost Devonian sequence - Sequence stratigraphy of the middle
572 Bakken member, and the importance of clastic dykes in the lower Bakken member shale,
573 North Dakota, USA: Marine and Petroleum Geology, v. 81, p. 278-293,
574 doi.org/10.1016/j.marpetgeo.2017.01.015

575

576 Egenhoff, S.O., Van Dolah, A., Jaffri, A., and Maletz, J., 2011, Facies architecture and
577 sequence stratigraphy of the Middle Bakken Member, Williston Basin, North Dakota, *in*
578 Robinson, L., LeFever, J., and Gaswirth, S., eds., Bakken–Three Forks Petroleum System in
579 the Williston Basin: Rocky Mountain Association of Geologists, Guidebook, p. 27–47 (on CD).

Ferdous, H., 2001, Regional sedimentology and diagenesis of the Middle Bakken member: Implications for reservoir rock distribution in southern Saskatchewan (Doctoral dissertation, University of Saskatchewan), 467 p.

Freisatz, W.B., 1995, Fracture-enhanced porosity and permeability trends in the Bakken Formation, Williston Basin, western North Dakota: 7th International Williston Basin Symposium, p. 389 - 398.

Gaines, A.M., 1974, Protodolomite synthesis at 100 C and atmospheric pressure: Science, v. 183, p. 518-520.

Giles, M.R. ed., 1997, Diagenesis: A Quantitative Perspective: Implications for Basin Modelling and Rock Property Prediction: Dordrecht, Kluwer Academic Publishers, 526p.

Giles, M.R., Indrelid, S.L., Beynon, G.V., and Amthor, J., 2000, The origin of large-scale quartz cementation: Evidence from large data sets and coupled heat-fluid mass transport modelling, *in* Worden, R.H., and Morad, S., eds., Quartz Cementation in Sandstones, International Association Sedimentologists, Special Publication, 29, p. 21-38.

600 Girard, J.P., Munz, I.A., Johansen, H., Hill, S., and Canham, A., 2001, Conditions and timing of
601 quartz cementation in Brent reservoirs, Hild Field, North Sea: constraints from fluid
602 inclusions and SIMS oxygen isotope microanalysis: Chemical Geology, v. 176, p. 73-92.

603

604 Goldstein, R.H., 2001, Fluid inclusions in sedimentary and diagenetic systems: Lithos, v. 55,
605 p. 159-193, doi.org/10.1016/S0024-4937(00)00044-X

606

607 Glasmann, J.R., Lundergard, P.D., Clark, R.A., Penny, B.K., and Collins, I.D., 1989,
608 Geochemical evidence for the history of diagenesis and fluid migration; Brent Sandstone,
609 Heather Field, North Sea: Clay Minerals, v. 24, p. 255-284.

610

611 Gluyas, J., and Coleman, M., 1992, Material flux and porosity changes during sediment
612 diagenesis: Nature, v. 356, p. 52-54.

613

614 Graham, C.M., Valley, J.W., and Winter, B.L., 1996, Ion microprobe analysis of $^{18}O/^{16}O$ in
615 authigenic and detrital quartz in the St. Peter Sandstone, Michigan Basin and Wisconsin
616 Arch, USA: contrasting diagenetic histories: Geochimica et Cosmochimica Acta, v. 60, p.
617 5101-5116.

618

619 Hart, B.S., Longstaffe, F.J., and Plint, A.G., 1992, Evidence for relative sea level change from
620 isotopic and elemental composition of siderite in the Cardium Formation, Rocky Mountain
621 Foothills: Bulletin of Canadian Petroleum Geology, v. 40, p. 52-59.

622

623 Harwood, J., Aplin, A.C., Fialips, C.I., Iliffe, J.E., Kozdon, R., Ushikubo, T., and Valley, J.W.,
624 2013, Quartz cementation history of sandstones revealed by high-resolution SIMS oxygen
625 isotope analysis: Journal of Sedimentary Research, v. 83, p. 522-530.

626

627 Haszeldine, R.S., Samson, I.M., and Cornford, C., 1984, Dating diagenesis in a petroleum
628 basin, a new fluid inclusion method: Nature, v. 307, p. 354-357.

629

630 Holland, F.D. Jr, Hayes, M.D., Thrasher, L.C., and Huber, T.P., 1987, Summary of the
631 biostratigraphy of the Bakken Formation (Devonian and Mississippian) in the Williston basin,
632 North Dakota: 5th International Williston Basin Symposium, p. 68 – 76.

633

634 Hudson, J.D., and Anderson, T.F., 1989, Ocean temperatures and isotopic compositions
635 through time: Royal Society of Edinburgh, Transactions, Earth Sciences, v. 80, p. 183-192.

636

637 Iampen, H.T., and Rostron, B.J., 2000, Hydrogeochemistry of pre-Mississippian brines,
638 Williston Basin, Canada-USA: Journal of Geochemical Exploration, v. 69, p. 29-35.

639

640 Kaczmarek, S.E., and Sibley, D.F., 2007, A comparison of nanometer-scale growth and
641 dissolution features on natural and synthetic dolomite crystals: implications for the origin of
642 dolomite: Journal of Sedimentary Research, v. 77, p. 424-432.

643

644 Karasinki, D.R., 2006, Sedimentology and hydrocarbon potential of the Devonian Three
645 Forks and Mississippian Bakken Formations, Sinclair Area, southeast Saskatchewan-
646 southwest Manitoba: Master's Dissertation, University of Manitoba, 436 p.

647

648 Kita, N.T., Ushikubo, T., Fu, B., and Valley, J.W., 2009, High precision SIMS oxygen isotope
649 analyses and the effect of sample topography: Chemical Geology, v. 264, p. 43-57.

650

651 Klein, J.S., Mozley, P., Campbell, A., and Cole, R., 1999, Spatial distribution of carbon and
652 oxygen isotopes in laterally extensive carbonate-cemented layers: implications for mode of
653 growth and subsurface identification: Journal of Sedimentary Research, v. 69, p. 184-201.

654

655 Kozdon, R., Ushikubo, T., Kita, N.T., Spicuzza, M., and Valley, J.W., 2009, Intratest oxygen
656 isotope variability in the planktonic foraminifer *N. pachyderma*: Real vs. apparent vital
657 effects by ion microprobe: Chemical Geology, v. 258, p. 327-337.

658

659 Kuhn, P.P., Di Primio, R., Hill, R., Lawrence, J.R., and Horsfield, B., 2012, Three-dimensional
660 modeling study of the low-permeability petroleum system of the Bakken
661 Formation: American Association of Petroleum Geologists, Bulletin, v. 96, p. 1867-1897.

662

663 Land, L.S., Milliken, K.L., and Mcbride, E.F., 1987, Diagenetic evolution of Cenozoic
664 sandstones, Gulf of Mexico sedimentary basin: Sedimentary Geology, v. 50, p. 195-225.

665

666 Last, W., and Edwards, W., 1991, Petrology of the Middle Bakken Member in the Daly Field,
667 southwestern Manitoba: 6th International Williston Basin Symposium, p. 64-69.

668

669 Lee, M., and Savin, S.M., 1985, Isolation of diagenetic overgrowths on quartz sand grains for
670 oxygen isotopic analysis: Geochimica et Cosmochimica Acta, v. 49, p. 497-501.

671

672 Li, H., Hart, B., Dawson, M., and Radjef, E., 2015, Characterizing the Middle Bakken:
673 laboratory measurement and rock typing of the Middle Bakken Formation: URTeC 217485,
674 13 p.

675

676 Linzmeier, B.J., Kozdon, R., Peters, S.E., and Valley J.W., 2016, Oxygen isotope variability
677 within growth bands suggests daily depth migration behavior is recorded in Nautilus shell
678 aragonite: PLOS One, p. 1-31. DOI:10.1371/journal.pone.0153890

679

680 Lyon, I.C., Burley, S.D., Mckeever, P.J., Saxton, J.M., and Macaulay, C., 2000, Oxygen isotope
681 analysis of authigenic quartz in sandstones; a comparison of ion microprobe and
682 conventional analytical techniques, *in* Worden, R.H. and Morad, S., eds., Quartz
683 Cementation in Sandstones, International Association of Sedimentologists, Special
684 Publication, 29, p. 299-316.

685

686 Macaulay, C.I., Haszeldine, R.S., and Fallick, A.E., 1993, Distribution, chemistry, isotopic
687 composition and origin of diagenetic carbonates: Magnus Sandstone, North Sea: Journal of
688 Sedimentary Petrology, v. 63, p. 33-43.

689

690 Machel, H.G., 2004, Concepts and models of dolomitization: a critical reappraisal, *in*
691 Braithwaite, C. J. R., Rizzi, G. and Darke, G., eds., The Geometry and Petrogenesis of
692 Dolomite Hydrocarbon Reservoirs, Geological Society of, London, Special Publication, 235, p.
693 7-63.

694

695 Marchand, A.M., Macaulay, C.I., Haszeldine, R.S., and Fallick, A.E., 2002, Pore water
696 evolution in oilfield sandstones: constraints from oxygen isotope microanalyses of quartz
697 cement: Chemical Geology, v. 191, p. 285-304.

698

699 McBride, E.F., and Milliken, K.L., 2006, Giant calcite-cemented concretions, Dakota
700 Formation, central Kansas, USA: Sedimentology, v. 53, p. 1161-1179.

McCabe, H.R., 1959, Mississippian stratigraphy of Manitoba: Manitoba: Department of Mines and Natural Resources Mines Branch, Publication 58, 99 p.

Meissner, F., 1978, Petroleum geology of the Bakken Formation Williston basin, North Dakota and Montana, *in* The Economic Geology of the Williston Basin: Montana Geological Society 24th Annual Conference. Williston Basin Symposium, p. 207 - 227.

Meissner, F.F., 1991, Petroleum Geology of the Bakken Formation Williston Basin, North Dakota and Montana: Montana Geological Society. Guidebook to Geology and Horizontal Drilling of the Bakken Formation, p. 19 – 42.

Millán, M.I., Machel, H., and Bernasconi, S.M., 2016, Constraining temperatures of formation and composition of dolomitizing fluids in the Upper Devonian Nisku Formation (Alberta, Canada) with clumped isotopes: Journal of Sedimentary Research, v. 86, p. 107-112.

Murray, R.C., and Lucia, F.J., 1967, Cause and control of dolomite distribution by rock selectivity: Geological Society of America Bulletin, v. 78, p. 21-36.

721 O'Neil, J.R., Clayton, R.N., and Mayeda, T.K., 1969, Oxygen isotope fractionation in divalent
722 metal carbonates: Journal of Chemical Physics, v. 51, p. 5547-5558.

723

724 Osborne, M., and Haszeldine, S., 1993, Evidence for resetting of fluid inclusion temperatures
725 from quartz cements in oilfields: Marine and Petroleum Geology, v. 10, p. 271-278.

726

727 Pitman, J.K., Price, L.C., and Lefever, J.A., 2001, Diagenesis and fracture development in the
728 Bakken Formation, Williston Basin: Implications for reservoir quality in the Middle
729 member [No. 1653]. US Department of the Interior, United States Geological Survey [USGS]
730 Professional Paper 1653, USGS, Denver, [November 2001], p. 19.

731

732 Pollington, A.D., Kozdon, R., and Valley, J.W., 2011, Evolution of quartz cementation during
733 burial of the Cambrian Mount Simon Sandstone, Illinois Basin: In situ microanalysis of
734 $\delta^{18}O$: Geology, v. 39, p. 1119-1122.

735

736 Robinson, A., and Gluyas, J., 1992, Model calculations of loss of porosity in sandstones as a
737 result of compaction and quartz cementation: Marine and Petroleum Geology, v. 9, p. 319-
738 323.

739

740 Rostron, B.J., and Holmden, C., 2003, Regional variations in oxygen isotopic compositions in
741 the Yeoman and Duperow aquifers, Williston basin (Canada-USA): Journal of Geochemical
742 Exploration, v. 78, p. 337-341.

743

744 Schmid, S., Worden, R.H., and Fisher, Q.J., 2004, Diagenesis and reservoir quality of the
745 Sherwood Sandstone (Triassic), Corrib field, Slyne basin, west of Ireland: Marine and
746 Petroleum Geology, v. 21, p. 299-315.

747

748 Sibley, D.F., 1982, The origin of common dolomite fabrics: clues from the Pliocene: Journal
749 of Sedimentary Petrology, v. 52, p. 1087-1100.

750

751 Sibley, D.F., and Gregg, J.M., 1987, Classification of dolomite rock textures: Journal of
752 Sedimentary Petrology, v. 57, p. 967-975.

753

754 Sibley, D.F., Dedoes, R. E., and Bartlett, T. R., 1987, Kinetics of dolomitization: Geology, v. 15,
755 p. 1112-1114.

756

757 Simenson, A., 2010, Depositional Facies and Petrophysical Analysis of the Bakken Formation,
758 Parshall Field, Mountrail County, North Dakota (Doctoral dissertation, Colorado School of
759 Mines), 190 p.

760

761 Śliwiński, M.G., Kitajima, K., Kozdon, R., Spicuzza, M.J., Fournelle, J.H., Denny, A., and Valley,
762 J.W., 2016a, Secondary ion mass spectrometry bias on isotope ratios in dolomite–ankerite,
763 Part I: $\delta^{18}O$ matrix effects: Geostandards and Geoanalytical Research, v. 40, p. 157-172.

764

765 Śliwiński, M.G., Kozdon, R., Kitajima, K., Denny, A., and Valley, J.W., 2016b, Microanalysis of
766 carbonate cement $\delta^{18}O$ in a CO_2-storage system seal: Insights into the diagenetic history of
767 the Eau Claire Formation (Upper Cambrian), Illinois Basin: American Association of
768 Petroleum Geologists, Bulletin, v. 100, p. 1003-1031.

769

770 Smith, M. G., and Bustin, R. M., 1996, Production and preservation of organic matter during
771 deposition of the Bakken Formation (Late Devonian and Early Mississippian), Williston
772 Basin: Palaeogeography, Palaeoclimatology, Palaeoecology, v. 142, p. 185-200.

773

774 Staruiala, A., Qing, H., Chi, G., Stern, R., and Petts, D., 2013, Dolomite petrography and
775 stable isotope geochemistry of the Bakken Formation, southeastern Saskatchewan, *in*
776 Summary of Investigations 2013, Volume 1, Saskatchewan Geological Survey, Saskatchewan
777 Ministry of the Economy, Miscellaneous Report 2013-4.1, Paper A-8, 10 p.

778

779 Sullivan, M.D., Macaulay, C.I., Fallick, A.E., and Haszeldine, R.S., 1997, Imported quartz
780 cement in aeolian sandstone grew from water of uniform composition but has complex
781 zonation: Terra Nova, v. 9, p. 237-241.

782

783 Taylor, K.G., Gawthorpe, R.L., Curtis, C.D., Marshall, J.D., and Awwiller, D.N., 2000,
784 Carbonate cementation in a sequence-stratigraphic framework: Upper Cretaceous
785 sandstones, Book Cliffs, Utah-Colorado: Journal of Sedimentary Research, v. 70, p. 360-372.

786

787 Taylor, T.R., Giles, M.R., Hathon, L.A., Diggs, T.N., Braunsdorf, N.R., Birbiglia, G.V., Kittridge,
788 M.G., Macaulay, C.I., and Espejo, I.S., 2010, Sandstone diagenesis and reservoir quality
789 prediction: Models, myths, and reality: American Association of Petroleum Geologists,
790 Bulletin, v. 94, p. 1093-1132.

791

792 Vahrenkamp, V.C., and Swart, P.K., 1994, Late Cenozoic dolomites of the Bahamas:
793 Metastable analogues for the genesis of ancient platform dolomites, *in* Purser, B., Tucker M.
794 and Zenger, D., eds., Dolomites: A Volume in Honour of Dolomieu, International Association
795 of Sedimentologists, Special Publication, 21, p.133-153.

796

797 Valley, J.W., and Kita, N.T., 2009, *In situ* oxygen isotope geochemistry by ion microprobe, *in*
798 Fayek M., ed., Mineralogical Association of Canada Short Course: Secondary Ion Mass
799 Spectrometry in the Earth Sciences, v. 41, p. 19-63

800

Van Geldern, R., Joachimski, M.M., Day, J., Jansen, U., Alvarez, F., Yolkin, E.A., AND Ma, X.P., 2006, Carbon, oxygen and strontium isotope records of Devonian brachiopod shell calcite: Palaeogeography, Palaeoclimatology, Palaeoecology, v. 240, p. 47-67.

Vasconcelos, C., McKenzie, J.A., Warthmann, R., and Bernasconi, S.M., 2005, Calibration of the $\delta^{18}O$ paleothermometer for dolomite precipitated in microbial cultures and natural environments: Geology, v. 33, p. 317-320.

Warren, J., 2000, Dolomite: occurrence, evolution and economically important associations: Earth-Science Reviews, v. 52, p. 1-81.

Webster, R.L., 1984, Petroleum source rocks and stratigraphy of the Bakken Formation in North Dakota, *in* Woodward, J., Meissner, F.F., and Clayton, J.L., eds., Hydrocarbon Source Rocks of the Greater Rocky Mountain Region, Rocky Mountain Association of Geologists 1984 Symposium, p. 57-81.

Weyl, P.K., 1960, Porosity through dolomitization: conservation of mass requirements: Journal of Sedimentary Petrology, v. 30, p. 85–90.

820 Whitaker, F.F., and Xaio, Y., 2010, Reactive transport modeling of early burial dolomitization
821 of carbonate platforms by geothermal convection: American Association of Petroleum
822 Geologists, Bulletin, v. 94, p. 889-917.

823

824 Whitaker, F.F., Smart, P. L., and Jones, G.D., 2004, Dolomitization: from conceptual to
825 numerical models, *in* Braithwaite, C.J.R., Rizzi, G. and Darke, G., eds., The geometry and
826 petrogenesis of dolomite hydrocarbon reservoirs: Geological Society, London, Special
827 Publication, 235, p. 99-139.

828

829 Wilkinson, M., 1991, The concretions of the Bearreraig Sandstone Formation: geometry and
830 geochemistry: Sedimentology, v. 38, p. 899-912.

831

832 Williams, L.B., Hervig, R.L., AND Bjørlykke, K., 1997, New evidence for the origin of quartz
833 cements in hydrocarbon reservoirs revealed by oxygen isotope microanalyses: Geochimica
834 et Cosmochimica Acta, v. 61, p. 2529-2538.

835

836 **ACKNOWLEDGEMENTS**

837 The authors are grateful to Statoil, who funded this work, and to the team at Wisconsin
838 SIMS Laboratory for their assistance. WiscSIMS is supported by the National Science
839 Foundation (EAR-1355590) and the University of Wisconsin-Madison. Our thanks are
840 extended to the team at Scottish Universities Environmental Research Centre (SUERC) for

841 assistance in obtaining bulk stable-isotope measurements. Thanks are also extended to KT
842 Geoservices for XRD analysis. We thank reviewers Tony Buono and Sven Egenhoff, and AE
843 Joe Macquaker, for their insightful comments, which focused and improved the manuscript.
844 John Southard's editing is also very much appreciated.

845

LIST OF FIGURES

Figure 1 - A) Map of northern USA and southern Canada showing states and provinces. ND – North Dakota. B) Map of North Dakota, showing the location of the well in this study and that modelled in the Kuhn et al. (2012) study. C) Burial history of the Williston Basin developed for the basin center in North Dakota. The temperature through time is overlaid. Cambr - Cambrian, Ordov - Ordovician, Sil - Silurian, Carbon - Carboniferous, Pal - Paleogene, N - Neogene, Up - Upper, Mi - Middle, Lo - Lower, Penn - Pennsylvanian, Mio - Miocene. From Kuhn et al. (2012).

Figure 2 - A) Stratigraphic column of the Devonian-Mississippian strata overlying and underlying the Bakken Formation. B) Generalized lithological log showing the principal sedimentary structures in each facies, adjacent to which are the gamma-ray (GR), neutron-porosity (NPHI) and density-porosity (DPHI) logs.

Figure 3 - Core photograph taken with UV light of a section of the Middle Bakken (facies D1). Fluorescing zones indicate oil-bearing sandstones and siltstones. Calcite-cemented sandstones correspond to segments of the core showing no or low fluorescence. Ticks on ruler represent 10 cm.

Figure 4 - A) Bioclasts (Bc) in calcite (Ca) cement, showing a range of taxa including brachiopods, crinoids and algal mats, viewed in XPL. B) Detrital quartz (Qz) grains floating in

a calcite (Ca)-cemented zone, viewed under optical microscope in XPL. C) Small-scale, local cementation by calcite (Ca) cement and replacement dolomites of several morphologies (Type 2 [T2], Type 5 [T5] and Type 6 [T6]) with an occasional detrital quartz (Qz) grain (BSEM). D) Larger-scale view of cementation of detrital quartz (Qz) grains by calcite (Ca) cement, viewed by SEM in BSE mode.

Figure 5 - Backscattered electron micrographs of the various textural types of diagenetic calcite identified in the Middle Bakken Formation. A) Type 1 calcite; forming a pervasive cement; B) Type 2 calcite; forming discrete grains, partially cementing other grains.

Figure 6 - Backscattered electron micrographs of the various textural types of dolomite identified in the Middle Bakken Formation. A) Type 1 - non-planar dolomite; B) Type 2 - planar-e with vuggy porosity; C) Type 3 - planar-e; D) Type 4 - planar-s; E) Type 5 - ferroan-dolomite rims around dolomite; F) Type 6 - planar-e (fine). In each case, D is the dolomite crystal of interest. Planar-e are euhedral dolomite, and planar-s are subhedral dolomite crystals (Sibley and Gregg, 1987).

885

886 **Figure 7** – SEM-CL spectra of the six different dolomite textures: A) Mixed SE-inline BSE image; B)
887 SEM-CL image; C) Averaged CL spectra (for each zone) with schematic sketch of the CL generations
888 and their relative luminescence [inset].

889

890 **Figure 8** – Ternary plot of the calcium, magnesium, and iron abundance in Middle Bakken
891 dolomites. A) All data; B) Type 1 dolomites; C) Type 2 (red) and Type 3 (blue) dolomites; D)
892 Type 4 dolomites; E) Type 6 dolomites. Type 7 dolomites were omitted due to their scarcity
893 and fine nature.

894

895 **Figure 9 –** A) Grain-scale oxygen isotope data collected by SIMS, differentiated by sample
896 [SIMS sample numbers S2-S7; see Table 1 for details of individual samples]. Calcite and
897 dolomite are separated for comparison. B) Grain-scale oxygen stable-isotope data collected
898 by SIMS for dolomite differentiated by textural types T1-T6 [Refer to Figure 6 for textural
899 types]. Oxygen isotope data are reported relative to VSMOW. Error bars (2 SD) are plotted
900 but are in most cases smaller than the data-point marker.

901

902 **Figure 10 -** Secondary electron micrographs showing positions of SIMS analyses. $\delta^{18}O_{SMOW}$
903 values are labelled for each analysis. A) Analysis pits ablated from dolomite (1 & 2) and
904 calcite (3), sample 2, sites 2-004 (1), 2-013 (2) and 2-081 (3) [Excluded due to a boundary
905 breach]. B) An analysis pit at the center of the dolomite crystal, sample 1, site 1-051. C) four
906 analysis pits; 2-4 were taken in a transect across a crystal of dolomite, sample 1, sites 1-073

907 (1), 1-071 (2), 1-071a (3) and 1-071b (4) [Note that analysis 1 was excluded from the dataset
908 due to a boundary break]. D) Analysis pits from three crystals of dolomite (1) and calcite (2,
909 3 and 4), sample 3, sites 3-033 (1), 3-022 (2), 3-026 (3), 3-021 (4). [Note that analyses 1 and
910 2 were excluded from the data set due to a boundary breaches]. Refer to Table 1 and
911 Supplementary Information for further information on each sample and individual sites.

912

913 **Figure 11** – Histogram of calculated precipitation temperatures from SIMS $\delta^{18}O$ values for:
914 A) Calcite, assuming $\delta^{18}O_{water}$ = -1.5‰; B) Dolomite, assuming $\delta^{18}O_{water}$ = -1.5‰; C)
915 Dolomite, assuming $\delta^{18}O_{water}$ = +3‰; D) Dolomite, assuming the $\delta^{18}O_{water}$ = +7.5‰.

916

917

Figure 1.

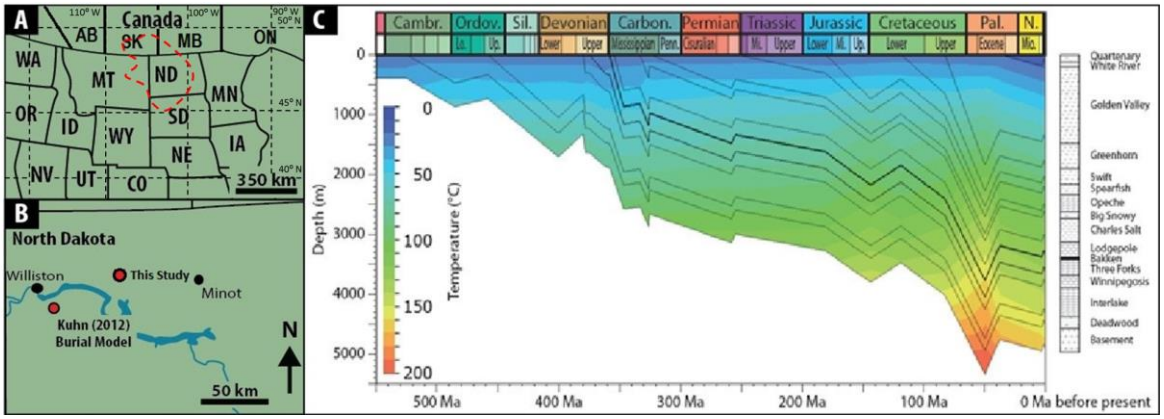
A
Canada
AB
SK
MB
ON
WA
MT
ND
MN
OR
ID
SD
WY
NE
IA
NV
UT
CO
350 km
B
North Dakota
Williston
This Study
Minot
Kuhn (2012)
Burial Model
50 km
N
C
Cambr.
Ordov.
Sil.
Devonian
Carbon.
Permian
Triassic
Jurassic
Cretaceous
Pal.
N.
Depth (m)
Temperature (°C)
500 Ma
400 Ma
300 Ma
200 Ma
100 Ma
0 Ma before present
Quartenary
White River
Golden Valley
Greenhorn
Swift
Spearfish
Opeche
Big Snowy
Charles Salt
Lodgepole
Bakken
Three Forks
Winnipegosis
Interlake
Deadwood
Basement

921 **Figure 2.**

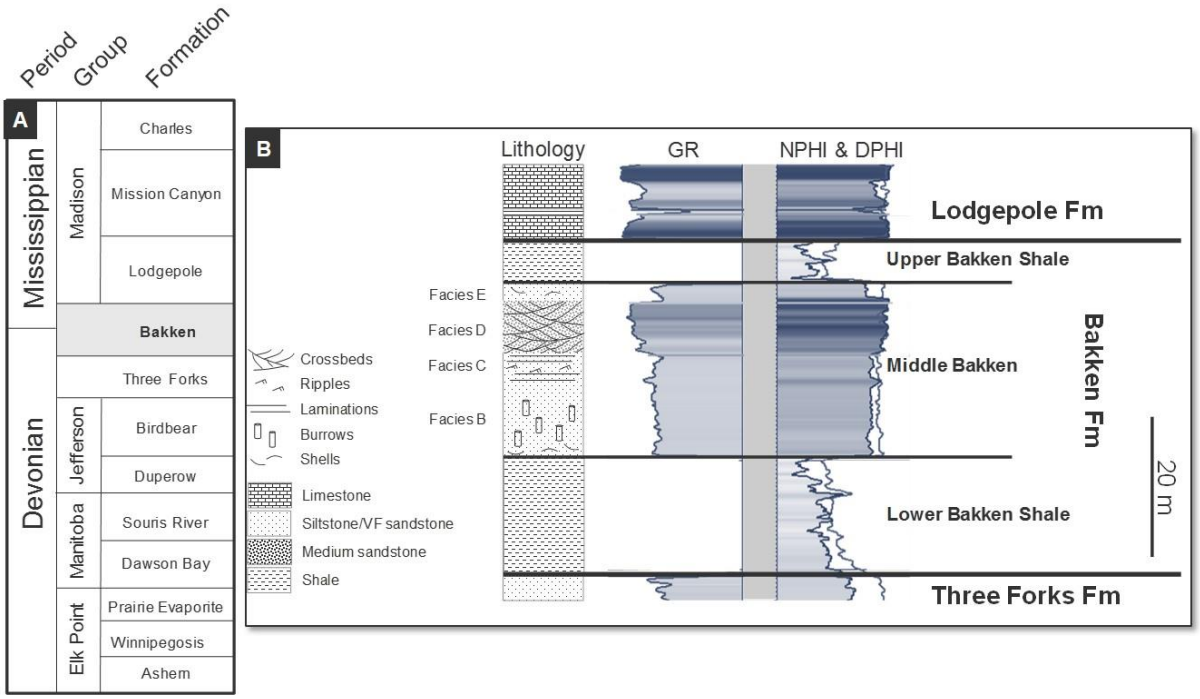

922

923

924 **Figure 3.**

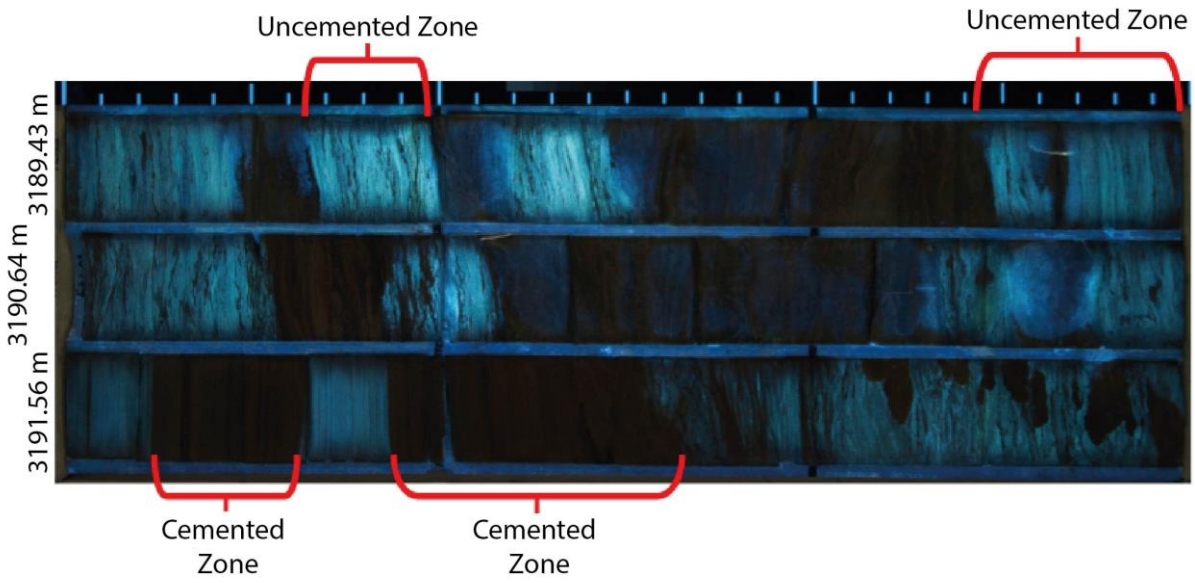

925

926

927 **Figure 4.**

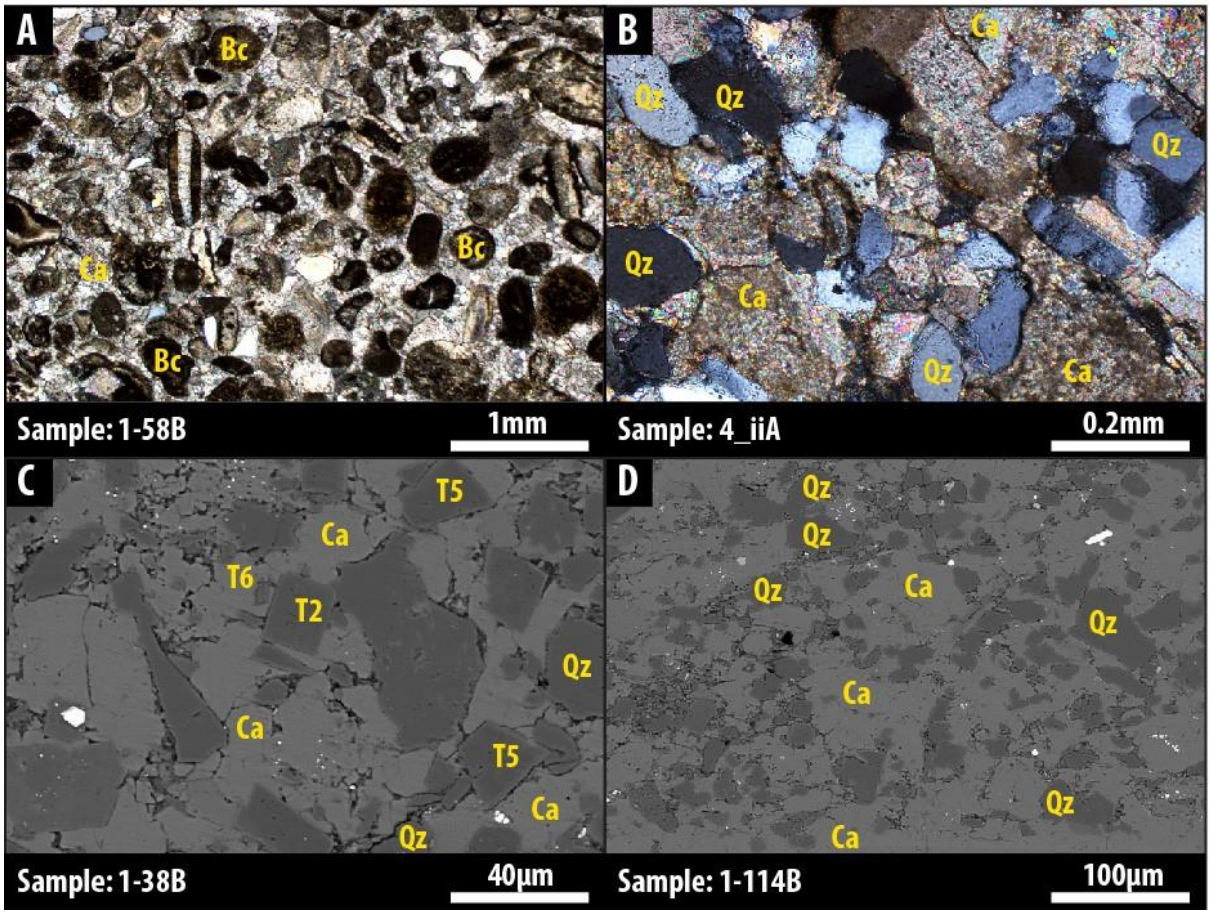

928

929

930 **Figure 5.**

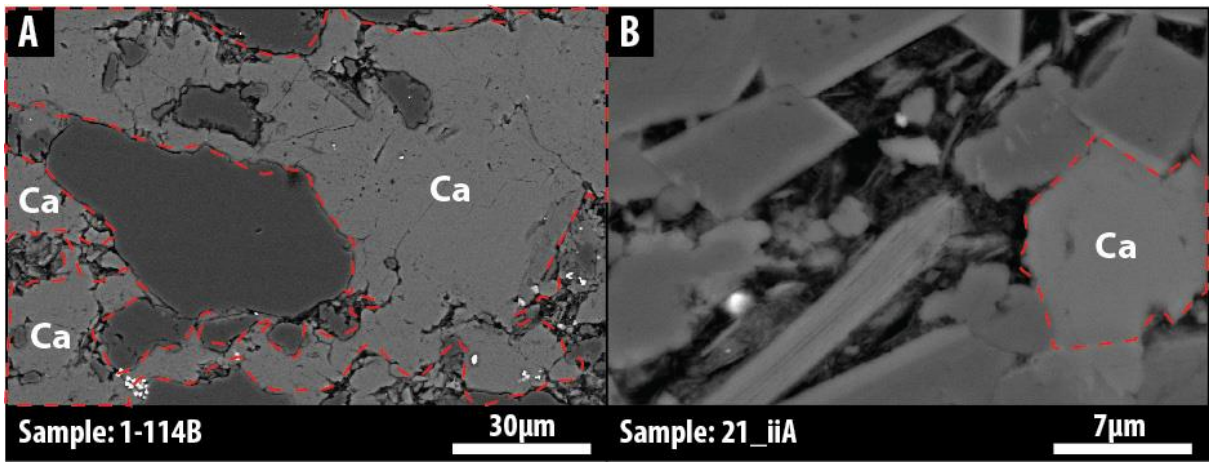

931

932

933 **Figure 6.**

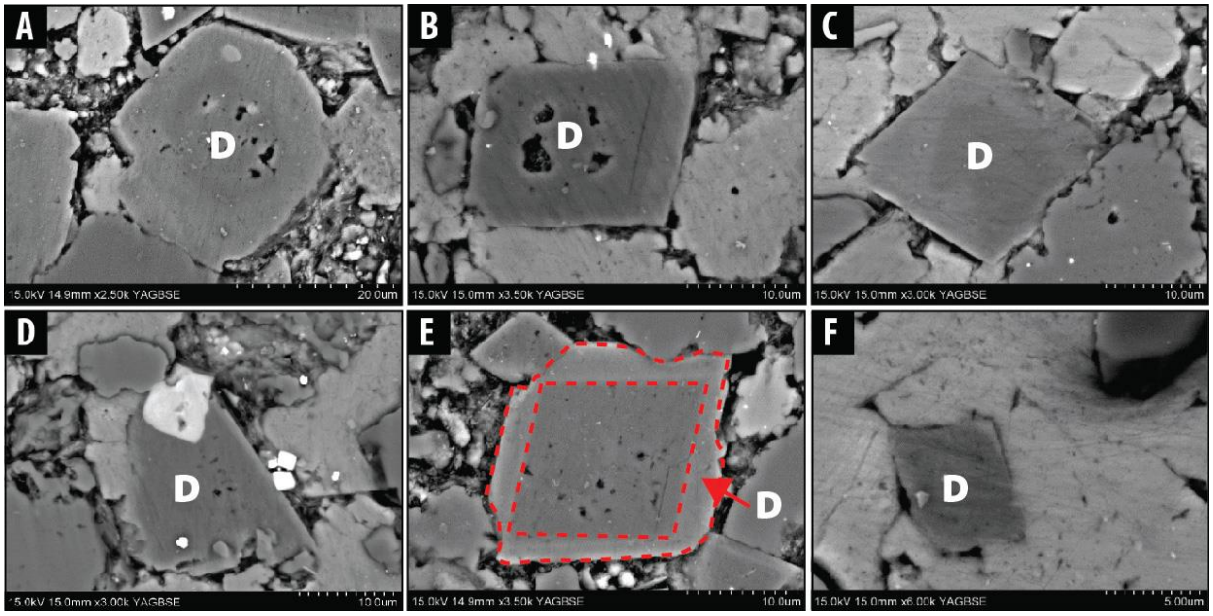

934

935

936 **Figure 7.**

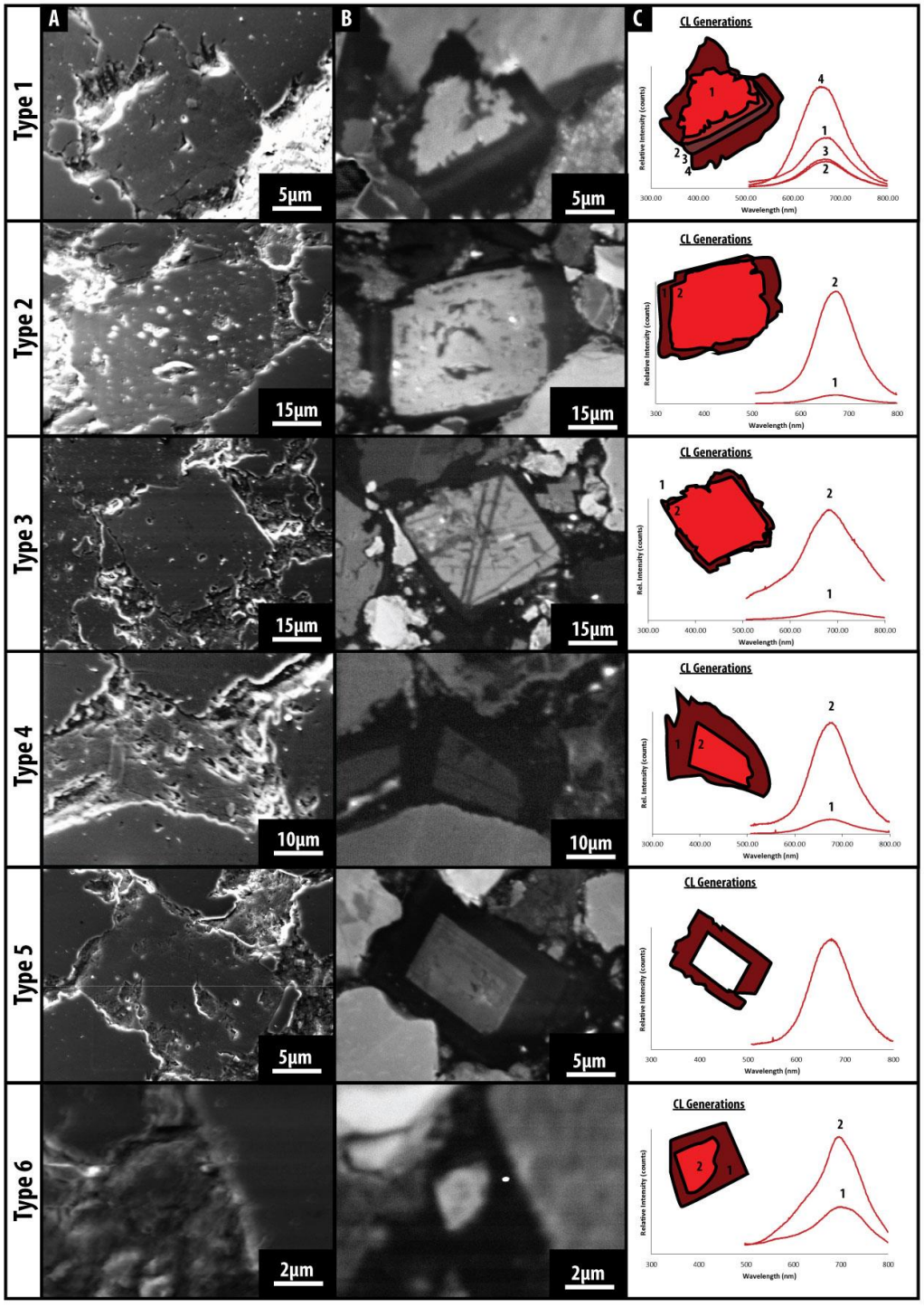

937

938

939 **Figure 8.**

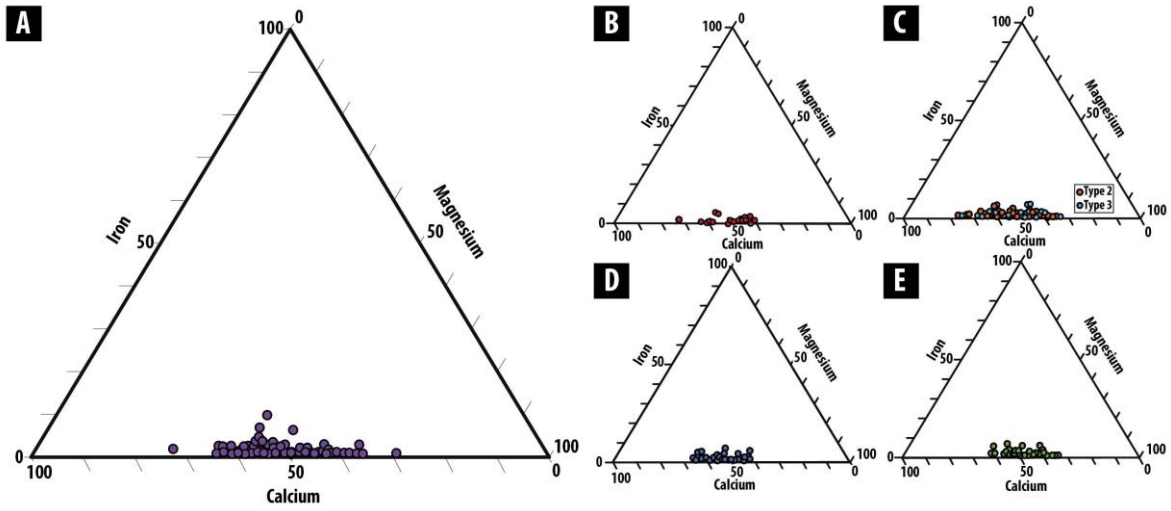

940

941

942 **Figure 9.**

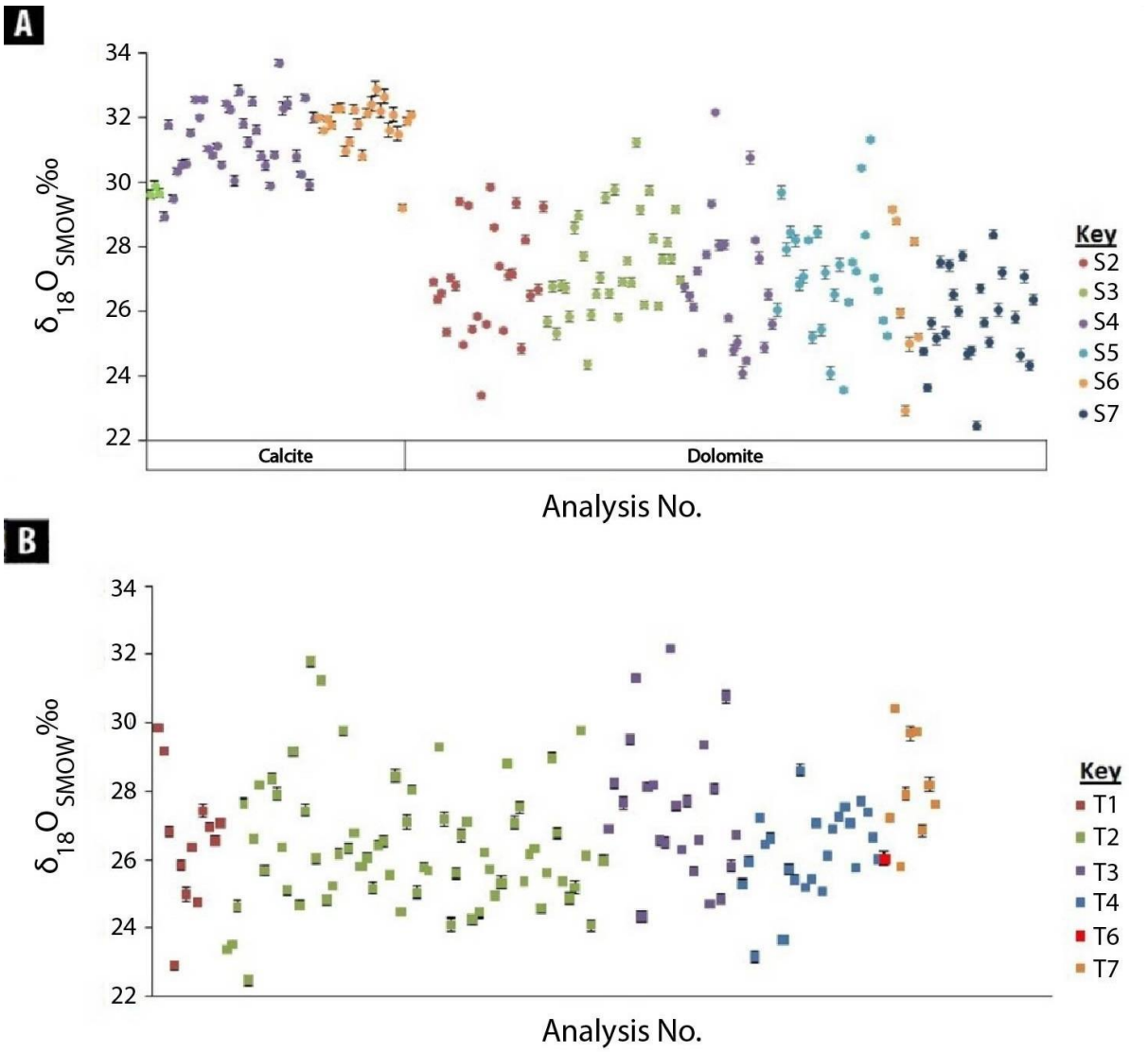

943

944

945 **Figure 10.**

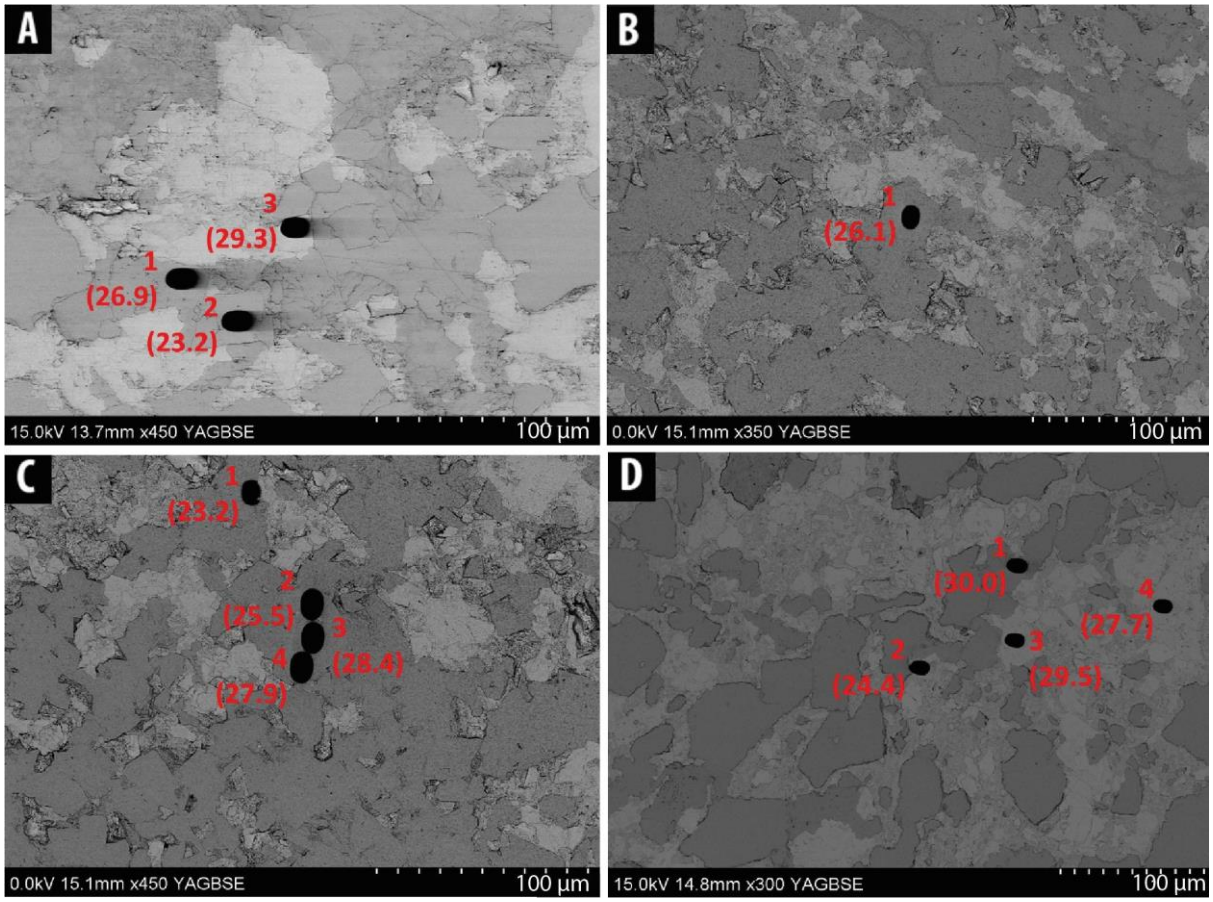

946

947

948 **Figure 11.**

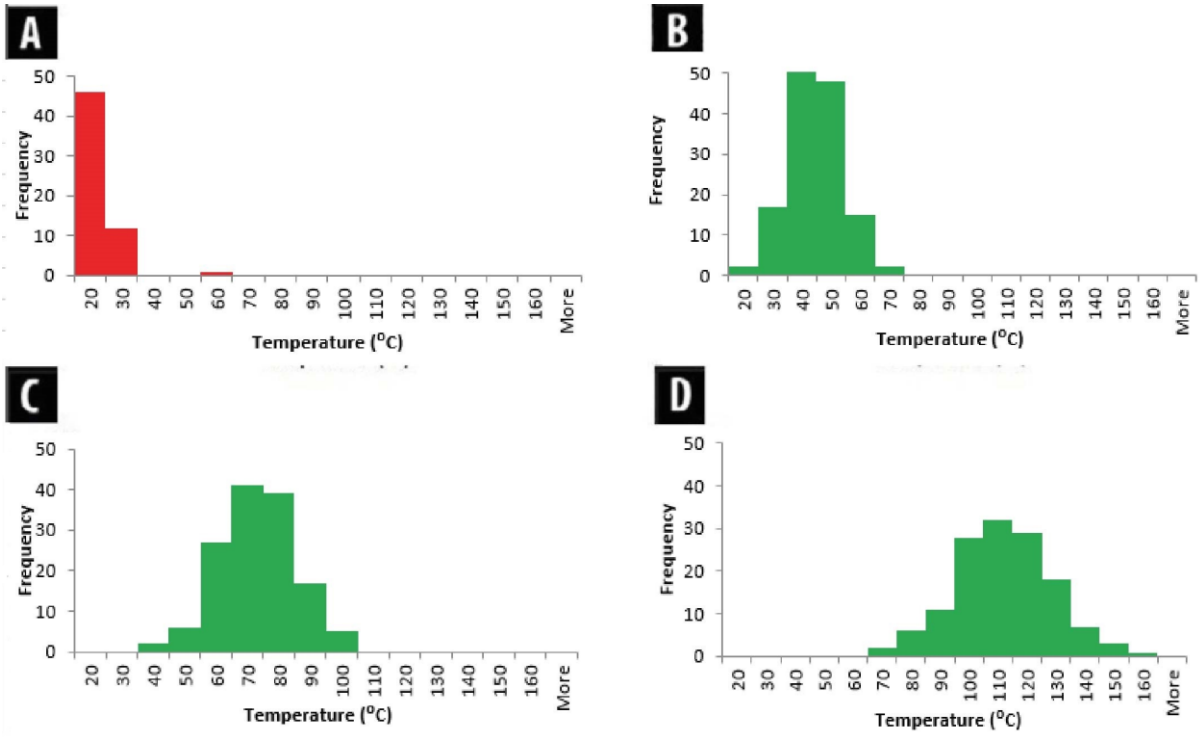

949

950

Table 1 – Mineralogical and bulk stable carbon and oxygen isotope data for calcite and dolomite obtained by sequential acid dissolution. Carbonate minerals calcite and dolomite were separated using conventional phosphoric acid digestion and gas-source mass spectrometric analyses on selected middle Bakken samples. Calcite is considered to be the CO_2 extracted after 3 hours of acid digestion at 25°C in a vacuum and dolomite is considered to be the CO_2 extracted after 24 hours at 100°C in a vacuum. Note that SIMS data from this study indicate that calcite and dolomite were not separated by this procedure. SIMS sample numbers are also shown.

Depth (m)	Sample No.	SIMS Sample No.	Facies	Oxygen and Carbon Isotopes by Sequential Acid Extraction				XRD Mineralogy (wt %)								
				Calcite @ 25°C		Dolomite @ 100°C										
				Carbon ($\delta^{13}C_{VPDB}$)	Oxygen ($\delta^{18}O_{VSMOW}$)	Carbon ($\delta^{13}C_{VPDB}$)	Oxygen ($\delta^{18}O_{VSMOW}$)	Quartz	Illite & Mica	Potassium Fspar	Plagioclase Fspar	Calcite	Dolomite	Pyrite	Halite	Chlorite
969.93	1-36B	7	E	-0.2	26.4	-0.5	25.7	42	13	4	5	3	29	2	2	0
970.02	1-37B	N/A	E	-0.8	26.1	-0.2	26.7	33	16	4	5	3	37	2	1	0
970.10	1-38B	N/A	E	-2.5	23.7	0.8	28.6	19	4	2	2	56	16	1	0	0
970.21	1-39B	N/A	E	-0.4	26.5	0.0	27.4	28	10	4	3	7	47	1	0	0
970.98	2_iiA	6	D2	3.1	25.8	1.5	28.7	46	3	4	2	31	14	1	0	0
971.00	4_iiA	5	D2	3.8	27.1	2.7	30.9	46	4	3	1	30	15	1	0	0
972.43	9_iiA	4	D1	3.3	26.0	3.6	30.8	38	5	6	3	36	12	0	0	0
973.95	17_iiA	3	C	2.0	24.4	-0.3	26.1	45	8	8	5	14	21	1	0	0
975.96	11_iiA	2	Grad	-0.5	25.3	-0.5	27.0	31	6	5	4	11	42	1	0	0
977.12	1-113B	N/A	B	-3.2	25.4	-3.3	26.5	18	11	4	3	21	41	1	1	1
977.17	1-114B	N/A	B	2.5	24.7	-2.1	19.8	29	12	4	3	37	12	2	0	1
977.27	1-115B	N/A	B	1.6	25.3	-0.3	26.1	23	10	3	3	53	5	3	0	1
977.36	1-116B	N/A	B	1.5	25.5	-0.3	27.1	30	13	4	3	36	9	3	0	1

- Supporting Online Material –

Geochemistry of calcite and dolomite in the Middle Bakken Formation, USA.

Mark Brodie[1], Andrew Aplin[1], Bruce Hart[2], Ian Orland[3], John Valley[3], Adrian Boyce[4]

[1]Department of Earth Sciences, Durham University, UK, DH1 3LE.

[2]Statoil, Austin, TX 78730, United States.

[3]Department of Geoscience, University of Wisconsin-Madison, WI, USA.

[4]SUERC, Rankine Avenue, East Kilbride, G75 0QF.

Ion Microprobe Analysis of Carbonate Minerals

In situ oxygen isotope data were acquired in the WiscSIMS Laboratory at the University of Wisconsin–Madison by a CAMECA IMS 1280 large-radius multicollector ion microprobe (Kita et al., 2009, Valley and Kita 2009). Carbonate minerals calcite and dolomite were analyzed during four analytical sessions in October 2016 (**Error! Reference source not found.**). During the analytical sessions the $^{133}Cs^{+}$ primary ion beam had an intensity of ~1.2 nA generating a beam diameter of ~13 µm. The typical secondary $^{16}O^{-}$ ion intensity was ~$2.9x10^{9}$ cps. Measurements were performed in multi-collector Faraday Cup mode and with conditions similar to those reported by Kozdon et al. (2009). The secondary O^{-} ions ($^{16}O^{-}$, $^{16}O^{1}H^{-}$, $^{18}O^{-}$) were detected by Faraday cup. Charging of the sample surface was compensated by Au-coating and an electron flood gun. Grains of the University of Wisconsin calcite standard, UWC-3 [$\delta^{18}O$(VSMOW) of UWC-3 is 12.49‰ (±0.03‰ 1 SD, n= 9)] was mounted at the centre of sample mounted in the polished block (Kozdon et al., 2009). Four consecutive measurements of UWC-3 calcite standard were performed before and after every set of 8–17 sample analyses. The 2 SD of a set of bracketing standard analyses is assigned as the reproducibility of the bracketed sample analyses. Detailed analytical protocols are described in Kita et al. (2009).

Table X – Full details of SIMS & SEM-WDS analyses for individual crystals. Data not included in the plots and interpretation are also included to show the full bracketed analyses. External precision (reproducibility) is reported for each bracket. The 'Mineral/ Type/Comment' column gives details of the analysis including dolomite phase type as a number e.g. type 1 is '1', NF=Crystal was not found post-SIMS analysis, NC= Crystal was not composed of a carbonate mineral, Calcite = calcite crystal. What is "Er" type in that column? Can you annotate which Mass Biases were corrected using the calibration curve? Would it be possible/prudent to include the standard calibration measurements (up to you)?

No.	Sample ID	^{16}O (Gcps)	$\delta^{18}O$ ‰ measured	2SE (int.)	Mass Bias	$\delta^{18}O$ ‰ VSMOW	2SD (ext.)	OH/O	Mineral / Type / Comment	CaO	MgO	FeO
Sample Mount No. 2. 13 µm beam, 1.2 nA intensity. October 6th 2015												
1	2 UWC3 G1	2.99	5.22	0.45								
2	2 UWC3 G1	3	5.04	0.45								
3	2 UWC3 G1	3.01	5.19	0.53								
4	2 UWC3 G2	2.97	5.2	0.5								
5	2-004	3.14	14.29	0.47	-12.28	26.9	0.21	0.003	2	51.93	51.44	0
6	2-005	3.07	15.38	0.45			0.21	0.005	NF			
7	2-006	3.01	13.75	0.46	-12.28	26.36	0.21	0.001	1	54.93	53.06	0.7
8	2-007	2.01	7.94	0.27	-5.41	13.41	0.21	0.001	NC			
9	2-008	2.91	13.95	0.53	-12.28	26.56	0.21	0.002	3			
10	2 UWC3 G1		5.34	0.54								
11	2 UWC3 G1		5.34	0.47								
12	2 UWC3 G1		5.15	0.54								
13	2 UWC3 G1		5.13	0.56								
		Average:	**5.2**	**2SD:**	**0.21**							
14	2-009	2.15	7.02	0.22	-5.41	12.5	0.25	0.002		39.95	61.79	0.0
15	2-009-2	2.04	8.14	0.3	-5.41	13.63	0.25	0.004	NC			
16	2-009-3	2.12	10.04	0.23	-5.41	15.54	0.25	0.005	NC			
17	2-011	3.09	13.41	0.39	-11.64	25.35	0.25	0.005	2	36.69	63.31	0.5
18	2-012	3.07	14.41	0.71	-12.3	27.05	0.25	0.006	1	39.16	62.72	0.0
19	2-013	3.05	14.15	0.45	-12.3	26.78	0.25	0.008	2			
20	2-017	2.89	17.4	0.45	-11.64	29.39	0.25	0.004	3	39.98	61.04	0.6
21	2-018	2.07	7.9	0.29	-5.41	13.38	0.25	0.006	NC			
22	2-061	2.08	10.35	0.52	-5.41	15.85	0.25	0.006	NC			
23	2-021	2.09	7.01	0.32	-5.41	12.49	0.25	0.005	NC			

24	2 UWC3 G1	2.85	5.13	0.47								
25	2 UWC3 G1	2.81	5.29	0.5								
26	2 UWC3 G1	2.9	5.01	0.48								
27	2 UWC3 G1	2.96	5.08	0.47								
		Average:	**5.18**	**2SD:**	**0.25**							
28	2-022	3.19	13.42	0.49			0.18	0.006	NF			
29	2-022a	3.17	12.32	0.43	-12.33	24.96	0.18	0.002	2	41.56	59.51	0.1
30	2-022b	3.03	16.59	0.49	-12.33	29.28	0.18	0.002	2			
31	2-024	3.06	12.81	0.43	-12.33	25.46	0.18	0.003	4	38.9	61.14	0.1
32	2-025	3.05	13.18	0.5	-12.33	25.83	0.18	0.004	3	37.46	62.69	0.1
33	2-026	3.11	12.2	0.45	-10.93	23.38	0.18	0.001	2	43.13	56.1	1.1
34	2-027	2.08	15.05	0.28	-5.45	20.61	0.18	0.010	NF			
35	2-028	3.2	15.79	0.53	-9.57	25.6	0.18	0.002	2	39.87	69.81	2.9
36	2-028a	2.09	6.97	0.22	-5.45	12.48	0.18	0.001	NC			
37	2-029	3.01	18.6	0.49	-10.93	29.86	0.18	0.004	1	38.61	60.56	1.0
38	2 UWC3 G1	2.84	5.12	0.5								
39	2 UWC3 G1	2.82	5.13	0.57								
40	2 UWC3 G1	2.9	5.26	0.45								
41	2 UWC3 G1	2.93	5.17	0.45								
		Average:	**5.15**	**2SD:**	**0.18**							
42	2-030	2.99	14.99	0.38			0.14	**0.014**	NF			
43	2-031	3.19	18.44	0.53			0.14	0.014	NF			
44	2-032	2.98	14.85	0.5			0.14	0.014	NF			
45	2-033	3.12	15.97	0.39	-12.28	28.6	0.14	0.006	4	41.41	59.02	0.1
46	2-034	2.86	17.24	0.58			0.14	0.003	NF			

47	2-035	3.07	13.65	0.53			0.14	0.007	NF			
48	2-036	2.94	15.39	0.49			0.14	0.004	NF			
49	2-036$_a$	2.95	14.78	0.42	-12.28	27.39	0.14	0.004	4	42.72	57.84	1.7
50	2-038	3	12.82	0.57			0.14	0.005	NF			
51	2-039	3.02	12.82	0.52	-12.28	25.41	0.14	0.002	4	36.21	64.25	0.0
52	2 UWC3 G1	2.82	5.31	0.51								
53	2 UWC3 G1	2.8	5.27	0.58								
54	2 UWC3 G1	2.89	5.22	0.53								
55	2 UWC3 G1	2.94	5.16	0.49								
		Average:	**5.2**	**2SD:**								
56	2-040	3.12	14.48	0.52	-12.32	27.13	0.31	0.006	3	39.35	60.59	0.2
57	2-041	3.16	14.53	0.49			0.31	0.005	NF			
58	2-042	3.11	14.52	0.52	-12.32	27.18	0.31	0.002	3	36.17	63.79	0.3
59	2-043	3.04	15.06	0.49			0.31	0.004	NF			
60	2-043$_a$	3.03	16.69	0.39	-12.32	29.37	0.31	0.004	2	36.92	63	0.1
61	2-044	3.12	12.89	0.58	-11.66	24.84	0.31	0.002	3	40.59	59.44	0.6
62	2-045	3.06	13.27	0.45			0.31	0.003	NF			
63	2-046	2.95	15.55	0.43	-12.32	28.22	0.31	0.005	3	36.21	63.65	0.0
64	2-047	3.03	13.84	0.42	-12.32	26.49	0.31	0.002	3	36.81	63.64	0.0
65	2-048	2.98	15.19	0.43	-2.21	17.44	0.31	0.006	2	38.17	60.2	0.0
66	2-049	3.03	14.03	0.58	-12.32	26.68	0.31	0.002	3	39.55	61.79	0.1
67	2-081	2.72	16.58	0.49	-12.32	29.26	0.31	0.002	2	39.07	61.38	0.0
68	2 UWC3 G1	2.83	4.82	0.5								
69	2 UWC3 G1	2.82	5.27	0.49								
70	2 UWC3 G1; C_s 127-128	2.92	5.13	0.52								
71	2 UWC3 G1	2.96	5.13	0.53								

		Average:	**5.16**	**2SD:**	**0.31**							
Sample Mount No. 3. 13 µm beam, 1.2 nA intensity. October 6th 2015												
72	3 UWC3 G1	2.94	5.02	0.5								
73	3 UWC3 G1	2.94	5.1	0.52								
74	3 UWC3 G2	2.92	5.02	0.5								
75	3 UWC3 G2	2.89	5.31	0.49								
76	3-012	2.05	4.78	0.34	-5.4	10.23	0.33	0.001	NC			
77	3-015	2.94	14.77	0.77	-11.63	26.72	0.33	0.004	2	52.64	47.32	0.2
78	3-016	3.03	13.9	0.5	-11.63	25.83	0.33	0.001	1	51.65	48.27	0.4
79	3-017	3	16.62	0.49	-11.63	28.59	0.33	0.003	3	50.81	48.94	0.0
80	3 UWC3 G1	2.84	5.3	0.52								
81	3 UWC3 G1	2.83	5.49	0.56								
82	3 UWC3 G1	2.94	5.13	0.52								
83	3 UWC3 G1	2.95	5.18	0.49								
		Average:	**5.19**	**2SD:**	**0.33**							
84	3-018	3.19	16.43	0.41	-12.19	28.97	0.29	0.001	2	50.64	49.55	0.1
85	3-021	2.98	15.19	0.44	-12.19	27.71	0.29	0.003	4	53.39	46.96	0.1

86	3-022	2.98	12.54	0.43	-11.53	24.35	0.29	0.003	3	50.75	48.8	0.4
87	3-023	2.94	13.38	0.53	-12.19	25.88	0.29	0.005	2	50.85	49.03	0.0
88	3-024	2.87	14.03	0.39	-12.19	26.54	0.29	0.004	1	52.43	48.64	0.0
89	3-025	3.07	17.98	0.45	-8.83	27.04	0.29	0.002	4	53.58	44.76	0.0
90	3-026	2.65	16.98	0.54	-12.19	29.53	0.29	0.002	3	98.6	1.33	0.2
91	3-026$_a$	2.83	14.72	0.45	-11.53	26.55	0.29	0.003	3	51.79	49.36	0.6
92	3-027	2.72	17.22	0.42	-12.19	29.77	0.29	0.005	2	54.28	44.19	1.5
93	3 UWC3 G1	2.68	5.34	0.54								
94	3 UWC3 G1	2.68	5.51	0.5								
95	3 UWC3 G1	2.77	5.26	0.48								
96	3 UWC3 G1	2.91	5.18	0.5								
		Average:	**5.3**	**2SD:**	0.29							
97	3-028	3.06	13.29	0.54	-12.21	25.82	0.23	0.004	2	52.72	47.71	0.0
98	3-029	2.13	10.36	0.3	-5.32	15.77	0.23	0.008	NC			
99	3-030	2.02	11.45	0.28	-5.32	16.86	0.23	0.009	NC			
100	3-031	2.13	7.74	0.2	-5.32	13.14	0.23	0.001	NC			
101	3-032	3.23	14.37	0.53	-12.21	26.91	0.23	0.004	4	50.16	49.34	0.5
102	3-033	2.79	17.41	0.51			0.23	0.004	NF			
103	3-034	2.91	12.47	0.51			0.23	0.004	NF			

104	3-035	1.94	15.02	0.3	-5.32	20.45	0.23	0.001	NC			
105	3-036	2.94	12.58	0.43			0.23	0.004	NF			
106	3-037	3.08	15.2	0.52			0.23	0.005	NF			
107	3 UWC3 G1	2.88	5.19	0.53								
108	3 UWC3 G1	2.87	5.3	0.5								
109	3 UWC3 G1	2.87	5.16	0.43								
110	3 UWC3 G1	2.87	5.22	0.57								
		Average:	**5.27**	**2SD:**	**0.23**							
111	3-038	2.72	16.68	0.5			0.27	0.005	NF			
112	3-039	2.93	17.25	0.43			0.27	0.006	NF			
113	3-040	2.93	15.55	0.45			0.27	0.005	NF			
114	3-041	2.79	14.54	0.46			0.27	0.006	NF			
115	3-092	2.09	12.91	0.25	-5.31	18.32	0.27	0.001	NC			
116	3-093	3	15.58	0.48	-12.2	28.13	0.27	0.004	3	52.56	46.99	0.9
117	3-096	2.6	17.09	0.51	-12.2	29.66	0.27	0	2	98.55	1.16	0.2
118	3-097	2.87	15.09	0.55	-12.2	27.63	0.27	0.003	2	53.57	46.54	3.5
119	3 UWC3 G1	2.72	5.42	0.53								
120	3 UWC3 G1	2.69	5.55	0.5								

121	3 UWC3 G1; C_s 131-132	2.78	5.23	0.51								
122	3 UWC3 G1; C_s 132-133	2.94	5.18	0.41								
		Average:	**5.28**	**2SD:**	**0.27**							
126	3-098	3.29	16.62	0.47	-12.19	29.16	0.26	0.002	1	53.61	41.58	4.5
127	3-099	3.23	14.44	0.54	-12.19	26.95	0.26	0.020	1	50.64	47.75	1.7
128	3-091	2.82	17.36	0.54	-12.19	29.91	0.26	0.005	Calcite	97.25	2.54	0.1
129	3-090	3.19	15.1	0.44	-12.19	27.62	0.26	0.002	6	51.26	48.1	1.1
130	3-089	3.04	13.65	0.45	-12.19	26.15	0.26	0.005	2	65.33	36.39	0.2
131	3-088	3.06	15.73	0.57	-12.19	28.26	0.26	0.005	2	54.21	43.54	3.0
132	3-087	2.72	17.08	0.61	-12.19	29.63	0.26	0.003	Calcite	98.77	1.32	0.4
133	3-086	3.19	17.19	0.54	-12.19	29.74	0.26	0.002	6			
134	3-085	1.94	11.54	0.26	-5.3	16.93	0.26	0.001	NC			
135	3-084	2.02	9.39	0.2	-5.3	14.77	0.26	0.001	NC			
136	3-084$_a$	2.09	3.61	0.29	-5.3	8.95	0.26	0.000	NC			
137	3-084$_b$	3.03	13.8	0.46	-12.09	26.2	0.26	0.002	2	52.39	47.48	0.5
138	3-083	2.92	16.61	0.45	-12.19	29.15	0.26	0.003	2	51.34	49.07	0.6
139	3-081	2.97	15.22	0.51			0.26	0.004	3	49.49	50.29	0.0
140	3-080	2.98	15.04	0.57	-12.19	27.57	0.26	0.005	3	51.46	49.14	0.0
141	3-080$_a$	2.85	14.38	0.5	-12.19	26.89	0.26	0.004	3	54.12	45.84	0.1

142	3-080b	3.03	18.67	0.39	-12.19	31.23	0.26	0.004	2	53.89	44.37	2.8
143	3 UWC3 G1	2.76	5.18	0.47								
144	3 UWC3 G1	2.73	5.3	0.51								
145	3 UWC3 G1	2.72	5.27	0.38								
146	3 UWC3 G1	2.71	5.25	0.56								
		Average:	**5.3**	**2SD:**	**0.26**							
Sample Mount No. 4. 13 µm beam, 1.2 nA intensity. October 7th 2015												
147	4 UWC3 G1	2.84	5.03	0.5								
148	4 UWC3 G2	2.87	5.37	0.55								
149	4 UWC3 G2	2.86	5.34	0.52								
150	4 UWC3 G2	2.87	5.19	0.51								
151	4-004	2.87	16.29	0.54	-12.3	28.94	0.26	0.002	Calcite	99.41	0.59	0.0
152	4-005	2.97	14.11	0.56	-12.3	26.74	0.26	0.006	3	29.56	70.59	0.1
153	4-006	2.72	19.1	0.56	-12.3	31.79	0.26	0.003	2	96.84	3.53	0.0
154	4-007	3.12	14.52	0.33	-11.64	26.47	0.26	0.001	4	43.54	56.22	0.3
155	4-008	2.11	5.18	0.21	-5.41	10.65	0.26	0.000	NC			

156	4-009	2.94	13.49	0.58	-12.3	26.11	0.26	0.002	4	42.06	57.74	0.0
157	4-010	3.03	14.61	0.63	-12.3	27.25	0.26	0.003	4	40.07	59.27	0.6
158	4-011	2.54	19.26	0.42				0.004	Er	95.32	3.47	
159	4 UWC3 G2	2.83	5.1	0.56								
160	4 UWC3 G2	2.85	5.12	0.48								
161	4 UWC3 G2	2.86	5.27	0.52								
162	4 UWC3 G2	2.89	5.04	0.53								
		Average:	**5.19**	**2SD:**	**0.19**							
163	4-012	3.11	12.67	0.44	-11.75	24.71	0.22	0.008	3	40.07	59.27	0.6
164	4-013	2.9	16.72	0.45	-12.41	29.5	0.22	0.002	Calcite	96.74	0.9	1.1
165	4-014	2.81	17.56	0.53	-12.41	30.35	0.22	0.003	Calcite	97.44	1.78	0.3
166	4-015	3.12	15	0.44	-12.41	27.76	0.22	0.003	2	42.26	57.67	0.2
167	4-016	3.32	16.57	0.57	-12.41	29.34	0.22	0.003	3	42.62	57.56	0.3
168	4-017	2.84	17.77	0.71	-12.41	30.56	0.22	0.010	Calcite	96.72	3.11	0.6
169	4-018	2.94	17.81	0.54	-12.41	30.6	0.22	0.003	Calcite	94.79	2.96	1.0
170	4-018a	3	18.74	0.59	-12.41	31.54	0.22	0.003	Calcite	95.49	4.4	0.0
171	4 UWC3 G2	3.19	4.98	0.59								

172	4 UWC3 G2	3.2	5.14	0.45								
173	4 UWC3 G2	3.15	4.97	0.49								
174	4 UWC3 G2	3.12	4.95	0.48								
		Average:	**5.07**	**2SD:**	**0.22**							
175	4-019	3.04	19.71	0.52	-12.46	32.58	0.15	0.002	Calcite	96.63	3.63	0.1
176	4-020	2.98	19.16	0.53	-12.46	32.03	0.15	0.002	Calcite	98.56	3.27	0.0
177	4-021	2.95	19.71	0.51	-12.46	32.58	0.15	0.002	Calcite	98.64	3.09	0.0
178	4-022	2.8	18.2	0.57	-12.46	31.05	0.15	0.003	Calcite	97.4	3.76	0.4
179	4-023	3.09	18	0.46	-12.46	30.85	0.15	0.002	Calcite	97.83	2.69	0.0
180	4-024	3.05	20	0.48	-11.81	32.18	0.15	0.001	3	53.01	46.48	0.6
181	4-025	3.08	18.29	0.58	-12.46	31.14	0.15	0.004	Calcite	95.31	4.3	0.0
182	4-026	3.14	17.71	0.46	-12.46	30.56	0.15	0.002	Calcite	95.67	4.53	0.0
183	4 UWC3 G2	3.26	5.05	0.51								
184	4 UWC3 G2	3.28	4.91	0.47								
185	4 UWC3 G2	3.16	5.04	0.51								
186	4 UWC3 G2	3.14	5.08	0.44								
		Average:	**5.01**	**2SD:**	**0.15**							

187	4-027	2.96	19.61	0.51	-12.45	32.46	0.18	0.000	Calcite	96.81	3.25	0.0
188	4-066	2.92	18.52	0.48	-5.8	24.46	0.18	0.002	2			
189	4-074	2.95	17.43	0.45	-12.45	30.25	0.18	0.004	Calcite	92.15	7.51	0.0
190	4-074a	3.44	15.41	0.35	-12.45	28.21	0.18	0.001	3	29.05	72.06	0.0
191	4-074b	3.07	19.77	0.46	-12.45	32.62	0.18	0.003	Calcite	94.64	5.6	0.0
192	4-028	3.13	19.41	0.49	-12.45	32.26	0.18	0.001	Calcite	98.12	1.63	0.1
197	4 UWC3 G2	3.24	4.93	0.54								
198	4 UWC3 G2	3.25	5.01	0.54								
199	4 UWC3 G2	3.14	5.08	0.51								
200	4 UWC3 G2	3.01	5.19	0.5								
		Average:	**5.03**	**2SD:**	**0.18**							
201	4-029	2.89	17.35	0.56	-12.33	30.05	0.3	0.000	Calcite	97.09	2.66	0.2
202	4-030	2.81	20.11	0.44	-12.33	32.85	0.3	0.002	Calcite	95.89	4.69	0.0
203	4-031	3.03	15.37	0.42	-12.33	28.05	0.3	0.004	2	43.23	57.03	0.0
204	4-032	2.7	19.1	0.54	-12.33	31.83	0.3	0.004	Calcite	96.96	4.33	0.0
205	4-033	2.82	18.53	0.47	-12.33	31.25	0.3	0.003	Calcite	98.43	2.05	0.3
206	4-034	3.08	15.39	0.46	-12.33	28.07	0.3	0.003	3	43.63	56.02	0.0
207	4-035	2.91	19.78	0.49	-12.33	32.51	0.3	0.001	Calcite	98.43	2.62	0.0

208	4-035a	2.73	18.89	0.53	-12.33	31.61	0.3	0.004	Calcite	99.73	2.26	0.0
209	4-036	2.86	18.11	0.51	-12.33	30.82	0.3	0.001	Calcite	99.77	0	0.0
210	4 UWC3 G2	3.02	5.33	0.55								
211	4 UWC3 G2	3.05	5.18	0.45								
212	4 UWC3 G2	3.04	5.35	0.52								
213	4 UWC3 G2	3.06	5.11	0.47								
		Average:	**5.15**	**2SD:**	**0.3**							
Sample Mount No. 4. 13 µm beam, 1.2 nA intensity. October 7th 2015*												
214	4 UWC3 G2	3.09	5.3	0.46								
215	4 UWC3 G2	2.99	5.17	0.55								
216	4 UWC3 G2	2.95	5.16	0.53								
217	4 UWC3 G2	2.97	5.24	0.51								
218	4-038	2.16	4.78	0.23	-5.34	10.18	0.21	0.001	NC			
219	4-039	2.89	19.25	0.53	-6.37	25.78	0.21	0.001	6	95.97	3.56	0.0
220	4-048	2.89	17.3	0.46	-12.23	29.9	0.21	0.002	Calcite	99.15	0.89	0.5
221	4-051	2.74	18.27	0.48	-12.23	30.88	0.21	0.005	Calcite	98.53	1.41	0.5
222	4-056	2.38	21.05	0.54	-12.23	33.7	0.21	0.000	Calcite	95.62	3.99	0.2

223	4 UWC3 G2	2.69	5.49	0.51								
224	4 UWC3 G2	2.91	5.25	0.52								
225	4 UWC3 G2	3	5.19	0.47								
226	4 UWC3 G2	3.06	5.22	0.45								
		Average:	**5.25**	**2SD:**	**0.21**							
227	4-057	2.98	19.57	0.53	-12.32	32.29	0.38	0.000	Calcite	96.53	3.34	0.0
228	4-058	3.23	12.41	0.41	-12.32	25.04	0.38	0.008	2	41.6	59.03	0.0
229	4-059	2.98	19.76	0.58	-12.32	32.48	0.38	0.000	Calcite	96.4	2.72	0.4
230	4-061	3.22	12.15	0.43	-11.66	24.1	0.38	0.002	2	38.76	60.38	0.6
231	4-069	2.27	12.13	0.23	-5.43	17.66	0.38	0.000	NC			
232	4-069$_a$	3.23	12.25	0.46	-12.32	24.88	0.38	0.001	2	38.39	62.63	0.4
233	4-070	3.02	19.52	0.52	-10.92	30.77	0.38	0.001	3	97.11	3.82	0.1
234	4-072	3.02	18.12	0.55	-12.32	30.82	0.38	0.000	Calcite	95.66	2.9	1.3
235	4-078	3.28	14.99	0.5	-12.32	27.65	0.38	0.003	3	40.19	60.06	0.0
236	4-086	2.29	13.86	0.28	-5.43	19.4	0.38	0.003	NC			
237	4 UWC3 G2	3.09	5	0.4								
238	4 UWC3 G2	3.07	5.21	0.5								
239	4 UWC3 G2	3.11	5.08	0.5								

240	4 UWC3 G2	3.14	4.86	0.48								
		Average:	**5.16**	**2SD:**	**0.38**							
251	4-092	3.11	18.29	0.47	-12.33	31	0.32	0.002	Calcite	97.07	3.63	0.0
252	4-097	3.17	17.24	0.53	-12.33	29.94	0.32	0.002	Calcite	98.76	1.45	0.2
253	4-097a	3.11	19.27	0.52	-12.33	31.99	0.32	0.002	Calcite	97.3	3.08	0.2
254	4-089	3.53	13.63	0.49	-11.67	25.6	0.32	0.016	2	40.25	58.72	0.4
255	4-042; Cs 141-139	3.27	12.17	0.59	-12.33	24.81	0.32	0.003	2	41.28	58.44	0.3
256	4-043	2.93	17.82	0.59	-12.33	30.53	0.32	0.003		94.62	4.76	0.0
257	4-100	2.19	14.22	0.34	-5.44	19.77	0.32	0.009	NC			
258	4-082	3.31	12.92	0.58	-11.67	24.88	0.32	0.001	2	39.81	60.54	0.3
259	4-082a	3.26	13.87	0.57	-12.33	26.52	0.32	0.002	2	39.03	60.9	0.0
260	4 UWC3 G2	3.09	5.35	0.48								
261	4 UWC3 G2	3.09	5.28	0.51								
262	4 UWC3 G2	3.1	5.21	0.55								
263	4 UWC3 G2	3.12	5.23	0.57								
		Average:	**5.15**	**2SD:**	**0.32**							
Sample Mount No. 5. 13 µm beam, 1.2 nA intensity. October 8th 2015												

264	5 UWC3 G1	2.86	4.86	0.49								
265	5 UWC3 G2	2.89	4.96	0.5								
266	5 UWC3 G2	2.98	4.62	0.54								
267	5 UWC3 G2	2.99	4.82	0.46								
268	5-015	3.04	16.74	0.21	-12.57	29.69	0.39	0.004	6	52.16	46.54	1.2
269	5-015a	3.2	15	0.45	-12.57	27.92	0.39	0.004	6	50.99	48.25	1.0
270	5-015b	3.12	15.54	0.37	-12.57	28.46	0.39	0.004	6	50.41	48.45	1.0
271	5-015c	3.18	15.26	0.46	-12.57	28.19	0.39	0.005	6	51.26	47.73	1.1
272	5-089	2.12	9.08	0.32	-5.68	14.84	0.39	0.002	NC			
273	5-015d	3.16	13.94	0.62	-12.57	26.84	0.39	0.005	6	44.91	58.97	1.7
274	5-100	3.05	13.6	0.51	-12.57	26.51	0.39	0.009	3	52.34	47.53	0.0
275	5-100a	2.95	14.52	0.41	-12.57	27.43	0.39	0.007	1	50.27	48.1	1.3
276	5 UWC3 G1	2.8	5.27	0.48								
277	5 UWC3 G1	2.82	5.04	0.48								
278	5 UWC3 G1	2.98	4.92	0.48								
279	5 UWC3 G1	3.04	4.78	0.49								
		Average:	**4.91**	**2SD:**	**0.39**							

280	5-099	3.19	11.31	0.53	-12.47	24.08	0.39	0.002	2	51.59	48.66	0.0
281	5-098	3.12	14.4	0.5	-12.47	27.21	0.39	0.005	4	54.05	46.27	0.0
282	5-028	2.18	22.62	0.25	-5.58	28.36	0.39	0.002	NC			
283	5-028a	2.2	22.45	0.27	-5.58	28.19	0.39	0.002	NC			
284	5-028b	2.2	22.1	0.31	-5.58	27.84	0.39	0.002	NC			
285	5-023	3.12	14.29	0.35	-12.47	27.09	0.39	0.007	2	51.27	49.06	0.0
286	5-004	3.31	13.24	0.57	-12.47	26.03	0.39	0.009	5	50.91	47.78	1.8
287	5-005	2.18	8.78	0.3	-5.58	14.44	0.39	0.001	NC			
288	5-078	2.9	12.4	0.56	-12.47	25.18	0.39	0.004	2	51.05	48.85	0.2
289	5 UWC3 G1	2.59	4.94	0.51								
290	5 UWC3 G1	2.67	5.01	0.46								
291	~~5 UWC3 G1~~	~~2.89~~	~~1~~	~~10.72~~								
292	5 UWC3 G1	2.82	5.32	0.44								
293	5 UWC3 G1	2.87	4.81	0.54								
		Average:	**5.01**	**2SD:**	**0.39**							
294	5-080	2.93	15.67	0.47	-12.43	28.45	0.37	0.005	2	50.92	48.96	0.3
295	5-081	3	12.69	0.46	-12.43	25.43	0.37	0.002	4	51.83	47.53	0.5
296	5-082	2.1	11.3	0.25	-5.54	16.93	0.37	0.001	NC			

297	5-084	2.97	17.5	0.54			0.37	0.009	E_r			
298	5-053	1.86	10.58	0.27	-5.54	16.21	0.37	0.002	NC			
299	5 UWC3 G1	2.67	5.01	0.46								
300	5 UWC3 G1	2.75	5.07	0.51								
301	5 UWC3 G1	2.82	5.34	0.54								
302	5 UWC3 G1	2.87	4.94	0.46								
		Average:	**5.05**	**2SD:**	**0.37**							
Sample Mount No. 1. 13 µm beam, 1.2 nA intensity. October 8th 2015												
303	1 UWC3 G1	2.87	5.12	0.49								
304	1 UWC3 G1	2.9	5.01	0.46								
305	1 UWC3 G1	2.93	5.24	0.53								
306	1 UWC3 G1	2.93	4.87	0.47								
307	1-079	3	14.05	0.33	-12.56	26.95	0.39	0.006	3	49.35	48.35	1.6
308	1-073	3.11	11.75	0.52	-11.16	23.17	0.39	0.002	4	47.48	51.42	0.0
309	1-072	3.07	14.41	0.51	-12.56	27.32	0.39	0.002	2	49.43	50.23	0.7
310	1-071	3.14	12.58	0.47	-12.56	25.46	0.39	0.005	3	49.92	50.55	0.0
311	1-071$_a$	3.1	16.18	0.48	-11.9	28.42	0.39	0.005	2	46.15	53.38	0.3

312	1-071b	3.17	15.02	0.34	-12.56	27.93	0.39	0.004	2	48.36	51.38	0.7
313	1-074	3.24	13.91	0.51	-12.56	26.81	0.39	0.007	4	48.99	50.59	0.8
314	1-075	3.31	13.71	0.51	-11.9	25.93	0.39	0.004	4	45.64	54.67	0.0
315	1 UWC3 G1	3.17	4.91	0.5								
316	1 UWC3 G1	3.11	4.74	0.49								
317	1 UWC3 G1	2.98	4.74	0.46								
318	1 UWC3 G1	2.98	4.69	0.46								
		Average:	**4.92**	**2SD:**	**0.39**							
319	1-051	3.06	13.79	0.55	-11.96	26.06	0.28	0.004	2	47.21	52.91	0.5
320	1-051a	3.08	13.7	0.48	-10.5	24.46	0.28	0.006	2	46.63	53.15	1.9
321	1-051b	3.1	13.03	0.47	-12.61	25.98	0.28	0.007	2	47.02	53.07	0.0
322	1-052	3.13	13.37	0.55			0.28	0.008	Er			
323	1-053	3.15	11.64	0.47	-12.61	24.56	0.28	0.006	2	47.41	52.78	0.2
324	1-054	3.28	13.09	0.41	-12.61	26.03	0.28	0.002	2			
325	1-054a	3.23	13.23	0.5	-12.61	26.18	0.28	0.008	2	49.23	50.94	0.6
326	1-054b	3.2	12.84	0.44	-12.61	25.78	0.28	0.004	2	41.88	58.18	0.3
327	1-054c	3.16	12.66	0.46	-12.61	25.6	0.28	0.001	2	72.54	26.83	1.4
328	1-054d	3.11	13.95	0.46	-12.61	26.91	0.28	0.001	2	63.55	36	0.7

329	1 UWC3 G1	2.97	4.96	0.54								
330	1 UWC3 G1	3.03	4.8	0.56								
331	1 UWC3 G1	3.09	5	0.53								
332	1 UWC3 G1	3.14	5.07	0.52								
		Average:	**4.86**	**2SD:**	**0.28**							
333	1-067	3.33	13.28	0.59	-12.52	26.13	0.28	0.004	2	47.59	52.22	0.9
334	1-067$_a$	2.87	16.88	12.49	-12.52	29.78	0.28	0.006	2	49.33	50.53	0.2
335	1-067$_b$	3.09	13.57	0.66	-12.52	26.42	0.28	0.001	2	47.32	52.88	0.4
336	1-067$_c$	3.09	11.43	0.51	-12.52	24.25	0.28	0.008	2	48.78	52.04	0.0
337	1-067$_d$	3.07	14.91	0.45	-11.86	27.1	0.28	0.004	2	47.31	53.36	0.7
338	1-067$_e$	3.09	13.76	0.45	-12.52	26.61	0.28	0.007	2	48.51	52.41	1.9
339	1-067$_f$	3.07	12.72	0.49	-12.52	25.56	0.28	0.007	2	49.24	50.82	0.3
340	1-067$_g$	3.12	12.27	0.5	-12.52	25.11	0.28	0.002	2			
341	1 UWC3 G1	2.85	4.99	0.47								
342	1 UWC3 G1	2.83	5.18	0.54								
343	1 UWC3 G1	2.83	4.76	0.47								
344	1 UWC3 G1	2.8	4.9	0.56								

		Average:	**4.96**	**2SD:**	**0.28**							
Sample Mount No. 7. 13 µm beam, 1.2 nA intensity. October 8th 2015												
345	7 UWC3 G1	2.86	5.08	0.55								
346	7 UWC3 G1	2.88	5.12	0.51								
347	7 UWC3 G1	2.85	5.06	0.49								
348	7 UWC3 G1	2.8	5.09	0.53								
349	7 UWC3 G1	2.87	5.24	0.46								
350	7-004	3.25	12.67	0.45	-11.79	24.75	0.25	0.009	1	50.03	49.95	0.3
351	7-005	3.21	11.58	0.46	-11.79	23.65	0.25	0.010	4	51.22	48.5	0.6
352	7-006	2.25	7.01	0.3	-5.56	12.63	0.25	0.001	NC			
353	7-020	2.36	10.81	0.23	-5.56	16.46	0.25	0.001	NC			
354	7-021	2.11	7.22	0.3	-5.56	12.85	0.25	0.002	NC			
355	7-023	2.33	8.82	0.27	-5.56	14.45	0.25	0.001	NC			
356	7-024	2.33	12.7	0.32	-5.56	18.35	0.25	0.002	NC			
357	7-060	2.36	12.84	0.28	-5.56	18.5	0.25	0.001	NC			
358	7 UWC3 G1	3.23	4.79	0.51								
359	7 UWC3 G1	3.15	4.94	0.53								

360	7 UWC3 G1	3.03	4.97	0.39								
361	7 UWC3 G1	2.91	5.02	0.4								
		Average:	**5.04**	**2SD:**	**0.25**							
362	7-048	3.15	14.95	0.55	-12.43	27.72	0.33	**0.007**	3	52.67	45.85	0.0
363	7-047	3.1	13.24	0.48	-12.43	25.99	0.33	**0.007**	4	51.45	48.36	0.2
364	7-041	2.99	13.77	0.44	-12.43	26.53	0.33	**0.007**	3	51.87	48.16	0.1
365	7-041 a	1.96	5.55	0.26	-5.54	11.15	0.33	**0.002**	NC			
366	7-040	2.09	13.5	0.37	-5.54	19.15	0.33	**0.002**	NC			
367	7-100	2.94	13.59	0.44	-12.43	26.34	0.33	**0.008**	2	51.3	49.63	0.0
368	7-099	3.03	11.6	0.57	-12.43	24.33	0.33	**0.010**	3	52.11	48.4	0.0
369	7-098	2.13	7.3	0.25	-5.54	12.91	0.33	**0.003**	NC			
370	7 UWC3 G1	2.86	5.18	0.45								
371	7 UWC3 G1	2.85	5.05	0.51								
372	7 UWC3 G1	2.87	5.34	0.53								
373	7 UWC3 G1	2.91	5.11	0.48								
		Average:	**5.05**	**2SD:**	**0.33**							
374	7-051	3.08	12.17	0.52	-12.21	24.68	0.3	0.006	2	51.48	47.95	0.0

375	7-052	3.12	12.95	0.49	-11.56	24.79	0.3	0.008	3	52.16	47.27	0.3
376	7-053	1.99	9.81	0.27	-5.32	15.21	0.3	0.001	NC			
377	7-054	2.79	14.44	0.5	-7.84	22.46	0.3	0.008	2	55.27	42.11	3.1
378	7-054$_a$	1.85	15.6	0.43	-10.81	26.7	0.3	0.009	3	51.3	48.99	0.8
379	7-054$_b$	2.74	13.13	0.39	-12.21	25.65	0.3	0.013	3	50.63	49.74	0.0
380	7-055	2.85	12.52	0.48	-12.21	25.03	0.3	0.007	4	50.19	50.04	0.0
381	7-070	2.76	15.81	0.55	-12.21	28.37	0.3	0.008	2	50.96	50.03	0.6
382	7 UWC3 G1	2.62	5.43	0.53								
383	7 UWC3 G1	2.62	5.4	0.5								
384	7 UWC3 G1	2.71	5.43	0.56								
385	7 UWC3 G1	2.8	5.23	0.49								
		Average:	**5.27**	**2SD:**	**0.3**							
386	7-073	3.14	13.47	0.35	-12.25	26.04	0.38	0.007	2	47.49	49.76	0.9
387	7-074	3.09	14.61	0.53	-12.25	27.18	0.38	0.007	2	50.75	48.8	0.1
388	7-075	3.09	14.56	0.45	-1.82	16.41	0.38	0.008	3	48.46	53.53	0.0
389	7-079	2.8	15.72	0.44	-2.2	17.96	0.38	0.005	Calcite	95.53	3.75	0.2
390	7-080	3.07	13.25	0.45	-12.25	25.82	0.38	0.008	3	52.44	47.75	0.3
391	7-081	3.01	13.53	0.51	-10.84	24.64	0.38	0.010	2	50.13	49.45	0.2

392	7-081a	3.08	14.5	0.49	-12.25	27.08	0.38	0.007	2	53.33	47.05	0.0
393	7-081b	2.15	8.3	0.32	-5.36	13.73	0.38	0.006	NC			
394	7-082	2.15	8.3	0.32	-5.36	13.73	0.38	0.004	NC			
395	7 UWC3 G1;	2.89	5.04	0.53								
396	7 UWC3 G1;	2.98	5.35	0.43								
397	7 UWC3 G1;	3.01	5.01	0.54								
398	7 UWC3 G1;	2.99	5.03	0.47								
		Average:	**5.24**	**2SD:**	**0.38**							
399	7-029	2.23	8.28	0.26	-5.61	13.97	0.36	0.001		52.97	46.78	0.0
400	7-030	3.14	12.81	0.45	-12.5	25.63	0.36	0.009	2	52.12	47.92	0.1
401	7-037	3.23	12.34	0.47	-12.5	25.15	0.36	0.006	2	50.16	49.93	0.2
402	7-037a	3.29	15.37	0.4	-11.84	27.54	0.36	0.007	2	53.05	46.55	0.4
403	7-038	3.24	12.51	0.63	-12.5	25.33	0.36	0.006	2	50.6	49.28	0.1
404	7-038a	3.33	14.59	0.51	-12.5	27.44	0.36	0.010	2	53.44	46.08	0.2
405	7-043	0.02	32.95	26.24	NA	NA	NA	0.277	NC			
406	7-044	2.18	17.09	0.21	-5.61	22.83	0.36	0.002	NC			
407	7 UWC3 G1	3	4.73	0.48								

408	7 UWC3 G1	3.04	4.89	0.49								
409	7 UWC3 G1	3.04	4.89	0.57								
410	7 UWC3 G1	3.1	4.9	0.48								
		Average:	**4.98**	**2SD:**	**0.36**							
Sample Mount No. 6. 13 µm beam, 1.2 nA intensity. October 9th 2015												
411	6 UWC3 G1	2.75	5.16	0.44								
412	6 UWC3 G1	2.83	5.16	0.54								
413	6 UWC3 G1	2.87	5.13	0.48								
414	6 UWC3 G1	2.88	4.96	0.5								
415	6-004	2.12	8.21	0.26	-5.49	13.78	0.16	0.001	NC			
416	6-005	2.76	19.24	0.63	-12.38	32.02	0.16	0.005	Calcite	97.35	2.28	0.5
417	6-005a	3.05	16.42	0.41	-12.38	29.16	0.16	0.005	2	46.14	54.16	0.3
418	6-006	3.16	16.05	0.46	-12.38	28.78	0.16	0.005	2			
419	6-007	2.74	18.85	0.53	-12.38	31.62	0.16	0.002	4	44.92	51.46	3.5
420	6-009	2.83	19.19	0.55	-12.38	31.97	0.16	0.004	Calcite	97.41	2.32	0.4
421	6-010	2.83	19.19	0.55	-12.38	31.97	0.16	0.001	Calcite	96.3	3.06	0.3
422	6-027	0.01	-35.46	38.45	NA	NA	NA	0.213	Er			

423	6 UWC3 G1	2.83	5.01	0.52								
424	6 UWC3 G1	2.79	5.1	0.53								
425	6 UWC3 G1	2.79	5.2	0.58								
426	6 UWC3 G1	2.78	5.09	0.51								
427	6-027$_a$	0.07	-1.13	8.49	NA	NA	NA	0.074	E_r			
428	6-027$_b$	2.33	19.17	0.54	NA	NA	NA	0.006	E_r			
429	6-027$_c$	0.03	-3.65	20.26	NA	NA	NA	0.136	E_r			
430	6-028	2.94	12.21	0.46			0.25	0.007	NF			
431	6-029	2.62	18.95	0.53	-12.42	31.77	0.25	0.007	Calcite			
432	6-030	2.67	19.48	0.55	-12.42	32.3	0.25	0.004	Calcite	97.3	2.61	0.4
433	6-031	2.59	19.49	0.64	-12.42	32.31	0.25	0.006	Calcite	98.08	1.73	0.0
434	6 UWC3 G1	2.72	5.16	0.54								
435	6 UWC3 G1	2.8	5.15	0.41								
436	6 UWC3 G1	2.96	4.81	0.47								
437	6 UWC3 G1	2.99	4.97	0.52								
		Average:	**5.1**	**2SD:**	**0.16**							

438	6-032	2.77	18.05	0.46	-12.53	30.97	0.3	0.004	Calcite	96.66	2.66	0.2
439	6-033	2.94	18.35	0.48	-12.53	31.27	0.3	0.004	Calcite	97.25	2.63	0.3
440	6-034	2.86	19.34	0.55	-12.53	32.27	0.3	0.007	Calcite	98.25	2.45	0.1
441	6-035	2.91	18.89	0.57	-12.53	31.81	0.3	0.004	Calcite	97.96	2.7	0.0
442	6-036	3.36	15.93	0.48	-9.76	25.94	0.3	0.002	3	42.99	54.48	2.1
443	6-037	3.27	12.93	0.48	-9.76	22.91	0.3	0.003	1	45.89	53.17	2.1
444	6-038	2.87	17.93	0.54	-12.53	30.84	0.3	0.004	Calcite	97.27	2.84	0.0
445	6-039	2.88	19.21	0.49	-12.53	32.14	0.3	0.005	Calcite	99.17	1.35	0.1
446	6 UWC3 G1	2.97	4.87	0.5								
447	6 UWC3 G1	2.96	4.88	0.48								
448	6 UWC3 G1	2.93	4.81	0.53								
		Average:	**4.95**	**2SD:**								
449	6-040	2.87	19.61	0.48	-12.42	32.44	0.43	0.002	Calcite	97.73	1.73	0.4
450	6-040$_a$	3.27	15.7	0.44	-9.06	24.99	0.43	0.002	1	46.2	54.03	0.4
451	6-059	2.83	20.08	0.48	-12.42	32.91	0.43	0.002	Calcite	97.93	2.05	0.1
452	6-059$_a$	2.82	19.4	0.6	-12.42	32.22	0.43	0.004	Calcite	99.09	1.33	0.0
453	6-059$_b$	2.76	19.83	0.53	-12.42	32.66	0.43	0.005	Calcite	99.13	0.73	0.3
454	6-062	2.81	18.8	0.48	-12.42	31.62	0.43	0.005	Calcite	97.93	2.06	0.1

455	6-063	2.8	19.29	0.53	-12.42	32.11	0.43	0.007	Calcite	98.45	1.99	0.0
456	6-064	2.83	18.69	0.52	-12.42	31.51	0.43	0.002	Calcite	99.27	0.9	0.0
457	6 UWC3 G1	2.84	5.4	0.54								
458	6 UWC3 G1	2.85	5.08	0.52								
459	6 UWC3 G1	2.84	5.11	0.59								
460	6 UWC3 G1	2.85	5.24	0.49								
		Average:	**5.06**	**2SD:**	**0.43**							
461	6-074	2.75	19.25	0.57	-12.25	31.89	0.22	0.003	Calcite	97.51	2.48	0.0
462	6-075	2.75	19.47	0.55	-5.6	25.21	0.22	0.004	4	43.6	54.03	0.4
463	6-075	2.75	19.47	0.55	-5.6	25.21	0.22	0.004	Cal rep site number	97.05	2.19	0.0
464	6-077	2	15.64	0.3	-5.36	21.12	0.22	0.001	NC			
465	6-077$_a$	1.99	15.96	0.3	-5.36	21.44	0.22	0.001	NC			
466	6-077$_b$	2.07	8.37	0.27	-5.36	13.81	0.22	0.001	NC			
467	6-077$_c$	2.06	8.66	0.3	-5.36	14.1	0.22	0.001	NC			
468	6-070	2.71	19.5	0.5			0.22	0.004	Er			
469	6-071	3.18	16.61	0.37	-12.25	29.22	0.22	0.002	Calcite	97.3	2.46	0.2
470	6-068	2.85	15.57	0.34	-12.25	28.17	0.22	0.006		42	58.55	0.0
471	6 UWC3 G1	2.78	5.23	0.49								

472	6 UWC3 G1	2.77	5.35	0.49								
473	6 UWC3 G1	2.76	5.17	0.54								
474	6 UWC3 G1	2.75	5.28	0.49								
		Average:	**5.23**	**2SD:**	**0.22**							
Sample Mount No. 1. 13 µm beam, 1.2 nA intensity. October 9th 2015												
475	1 UWC3 G1	2.98	5.29	0.53								
476	1 UWC3 G1	2.84	5.27	0.47								
477	1 UWC3 G1	2.78	5.19	0.5								
478	1 UWC3 G1	2.72	5.05	0.56								
479	1-084	2.8	13.06	0.6	-12.35	25.72	0.2	0.007	2	49.57	51.37	0.0
480	1-084a	2.88	14.37	0.64	-11.69	26.37	0.2	0.008	2	49.45	50.75	0.0
481	1-085	2.84	12.7	0.52	-12.35	25.35	0.2	0.008	2	50.05	49.94	0.0
482	1-101	2.76	13.95	0.58	-12.35	26.62	0.2	0.009	4	49.45	50.75	0.7
483	1-102	2.76	12.63	0.42	-12.35	25.29	0.2	0.005	4	47.69	56.15	1.4
484	1-103	2.81	13.7	0.5	-12.35	26.37	0.2	0.008	4	50.69	50.53	0.2
485	1-104	2.78	14.16	0.49			0.2	0.007	E_r			
486	1-105	2.99	14.47	0.4	-12.39	27.2	0.16	0.005	4	48.66	52.15	0.0
487	1-106	2.96	13.04	0.44	-12.39	25.74	0.16	0.008	4	48.85	50.37	1.0
488	1-107	2.95	12.36	0.57	-12.39	25.06	0.16	0.006	4	47.98	52.14	0.2

489	1-108	2.93	13.37	0.44	-12.39	26.08	0.16	0.007	2	49.88	54.21	0.2
490	1-109	2.93	12.97	0.46	-12.39	25.68	0.16	0.011	2	45.84	54.92	1.3
491	1-110	2.89	13.61	0.48	-12.39	26.32	0.16	0.008	3	47.54	52.23	0.0
492	1-111	2.01	14.2	0.21	-5.5	19.81	0.16	0.001	NC			
493	1-112	2.88	12.22	0.48			0.16	0.006	E_r			
494	1-113	2.84	13.6	0.38	-12.39	26.31	0.16	0.005	2	48.17	52	0.0
495	1 UWC3 G1	2.73	5.2	0.51								
496	1 UWC3 G1	2.66	5.12	0.75								
497	1 UWC3 G1	2.7	5.19	0.46								
498	1 UWC3 G1	2.9	4.94	0.48								
		Average:	**5.16**	**2SD:**	**0.23**							
499	1-114	3.19	12.61	0.46			0.41	0.006	E_r			
500	1-115	3.18	11.83	0.64			0.41	0.016	E_r			
501	1-116	3.15	14.19	0.44			0.41	0.007	E_r			
502	1-117	3.09	14.58	0.25			0.41	0.013	E_r			
503	1-118	3.22	11.11	0.66			0.41	0.021	E_r			
504	1-119	3.13	12.53	0.45			0.41	0.007	E_r			

505	1-120	3.17	11.81	0.55			0.41	0.008	E_r			
506	1-121	3.1	14.38	0.59			0.41	0.007	E_r			
507	1-122	3.13	13.47	0.5			0.41	0.006	E_r			
508	1 UWC3 G1	3.02	4.73	0.49								
509	1 UWC3 G1	2.99	4.97	0.56								
510	1 UWC3 G1	2.99	4.64	0.51								
511	1 UWC3 G1	2.96	4.97	0.54								
		Average:	**4.97**	**2SD:**	**0.41**							
Sample Mount No. 5. 13 µm beam, 1.2 nA intensity. October 9th 2015												
512	5 UWC3 G2	3.04	4.92	0.52								
513	5 UWC3 G2	3.01	5.11	0.5								
514	5 UWC3 G2	3	4.94	0.5								
515	5 UWC3 G2	2.97	5.08	0.52								
516	5-072	3.21	15.35	0.37	-12.49	28.19	0.16	0.003	2	49.75	50.2	0.0
517	5-101	2.09	10.6	0.38	-5.6	16.3	0.16	0.001	NC			
518	5-102	2.99	11.28	0.53	-11.98	23.55	0.16	0.008	2	52.3	47.7	0.0
519	5-103	3.06	13.83	0.45	-12.13	26.28	0.16	0.006	3	50.1	49.9	0.0
520	5-104	2.14	5.23	0.28	-5.6	10.89	0.16	0.001	NC			

521	5-105	2.08	3.69	0.28	-5.6	9.35	0.16	0.008	NC			
522	5-106	2.13	5.87	0.25	-5.6	11.54	0.16	0.001	NC			
523	5-107	2.94	14.7	0.54	-12.49	27.54	0.16	0.003	4	50.85	49.1	0.3
524	5 UWC3 G2	2.91	4.9	0.49								
525	5 UWC3 G2	2.91	4.99	0.47								
526	5 UWC3 G2	2.88	4.93	0.45								
527	5 UWC3 G2	2.89	5.03	0.43								
		Average:	**4.99**	**2SD:**	**0.16**							
528	5-108	2.86	14.6	0.35	-12.29	27.22	0.14	0.004	6	51.51	48.03	0.3
529	5-109	3.15	17.58	0.4	-12.48	30.44	0.14	0.001	6	50.8	46.54	6.9
530	5-110	2.08	5.64	0.23	-5.63	11.34	0.14	0.001	NC			
531	5-111	2.08	5.56	0.25	-5.63	11.26	0.14	0.001	NC			
532	5-112	2.08	5.8	0.27	-5.63	11.5	0.14	0.001	NC			
533	5-113	3.05	15.47	0.47	-12.52	28.35	0.14	0.002	2	52.16	44.41	3.2
534	5-114	3.01	18.42	0.37	-12.52	31.34	0.14	0.005	3	50.43	50.01	0.3
535	5-115	2.97	14.19	0.42	-12.52	27.05	0.14	0.002	4	52.3	47.98	0.1
536	5 UWC3 G2	2.82	5.01	0.45								

537	5 UWC3 G2	2.82	4.82	0.53								
538	5 UWC3 G2	2.82	4.97	0.58								
539	5 UWC3 G2	2.81	5.02	0.41								
		Average:	**4.96**	**2SD:**	**0.14**							
540	5-116	2.04	6.99	0.26	-5.63	12.7	0.14	0.001	NC			
541	5-117	2.96	13.78	0.55	-12.52	26.63	0.14	0.001	4	51.29	48.6	0.1
542	5-118	2.92	12.88	0.41	-12.52	25.73	0.14	0.003	4	51.06	49.43	0.5
543	5-119	1.96	8.79	0.2	-5.63	14.5	0.14	0.001	NC			
544	5-120	1.94	9.77	0.26	-5.63	15.49	0.14	0.001	NC			
545	5-121	1.93	9.88	0.27	-5.63	15.6	0.14	0.001	NC			
546	5-122	2.83	12.4	0.39	-12.52	25.23	0.14	0.003	2	50.52	49.59	**0.4**

991

992

993

994

995

996

997

Pit Analysis

After ion microprobe analysis a combination of Scanning Electron (SE), Back Scattered (BSE) microscopy and Wavelength Dispersive Spectroscopy (SEM-WDS) was used to relocate and characterise each individual pit. Pits with an irregular morphology were excluded. In this study 'pit irregularity' is defined as and includes pits which are positioned on cracks, spots which break into crystals and/or inclusions other than the target mineral and spots which overlap pores and vugs. Analyses which were not of calcite or dolomite were also excluded. Analyses were also excluded where the pit could not be found or the pit identity confirmed. An explanation each excluded analysis is given in Table X. In total 111 measurements were excluded from a total of 308 analyses

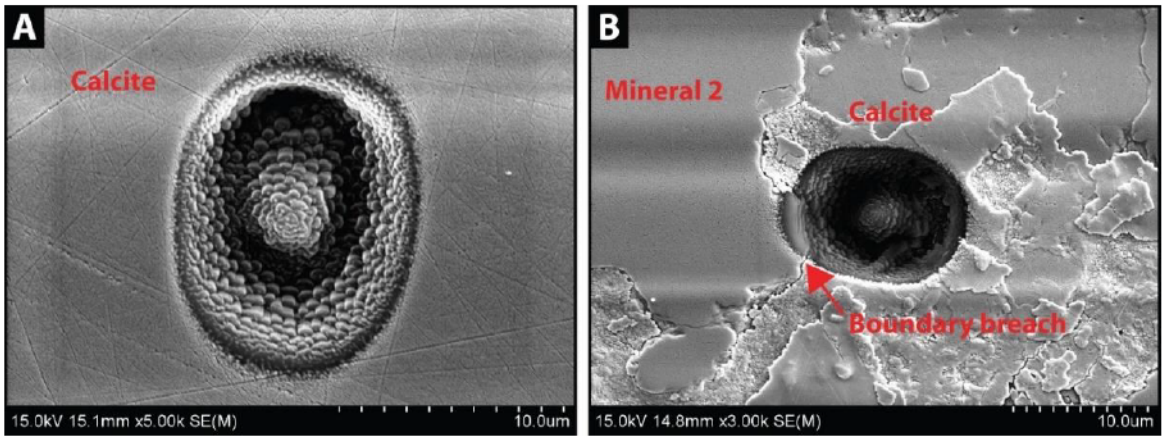

Figure X - Examples of SIMS pits a) Regular pit, positioned in the centre of a calcite crystal in sample 2-55B; note the ellipsoidal shape and size. Note, the pit is shown rotated 90° to the orientation it was created in; b) Irregular pit positioned at the edge of calcite cement, breaking into a second mineral (mineral 2), contaminating the ablated sample, in sample 2-55B.

Table X – Details of pits excluded from further interpretations. Not found = where the pit couldn't be located for integrity checking. Other Mineral = analyses of minerals other than calcite or dolomite and were commonly feldspar or quartz. Error = Refers to low count rates obtained by the detector.

Analysis ID	Explanation
1-051b	Irregularity
1-052	Error
1-054	Not Found
1-067g	Not Found
1-073	Irregularity
1-075	Irregularity
1-084a	Not Found
1-104	Error
1-111	Other Mineral
1-112	Error
1-114	Error
1-115	Error
1-116	Error
2-005	Not Found
2-007	Other Mineral
2-008	Not Found
2-009	Irregularity
2-009-2	Other Mineral
2-009-3	Other Mineral
2-013	Not Found
2-018	Other Mineral
2-021	Other Mineral
2-022	Not Found
2-022b	Not Found
2-027	Not Found
2-028a	Other Mineral
2-030	Not Found
2-031	Not Found

Analysis ID	Explanation
2-032	Not Found
2-034	Not Found
2-035	Not Found
2-036	Not Found
2-038	Not Found
2-041	Not Found
2-043	Not Found
2-045	Not Found
2-048	Irregularity
2-061	Other Mineral
3-006	Other Mineral
3-011	Other Mineral
3-012	Other Mineral
3-017	Irregularity
3-025	Irregularity
3-029	Other Mineral
3-030	Other Mineral
3-031	Other Mineral
3-033	Not Found
3-034	Not Found
3-035	Other Mineral
3-036	Not Found
3-037	Not Found
3-038	Not Found
3-039	Not Found
3-040	Not Found
3-041	Irregularity
3-081	Error

Analysis ID	Explanation
3-084	Other Mineral
3-084a	Other Mineral
3-085	Other Mineral
4-008	Other Mineral
4-011	Irregularity
4-038	Other Mineral
4-043	Irregularity
4-066	Not Found
4-069	Other Mineral
4-086	Other Mineral
4-100	Other Mineral
5-005	Other Mineral
5-028	Other Mineral
5-028a	Other Mineral
5-028b	Other Mineral
5-053	Other Mineral
5-082	Other Mineral
5-084	Error
5-089	Other Mineral
6-004	Other Mineral
6-006	Not Found
6-027	Error
6-027a	Error
6-027b	Error
6-027c	Error
6-028	NC
6-068	Irregularity
6-070	Error

Analysis ID	Explanation
6-075	Not Found
6-077	Other Mineral
3-086	Not Found
3-092	Other Mineral
6-077a	Other Mineral
6-077b	Other Mineral
6-077c	Other Mineral
7-006	Other Mineral
7-020	Other Mineral
7-021	Other Mineral
7-023	Other Mineral
7-024	Other Mineral
7-029	Irregularity
7-040	Other Mineral
7-041a	Other Mineral
7-043	Other Mineral
7-044	Other Mineral
7-048	Irregularity
7-051	Irregularity
7-053	Other Mineral
7-060	Other Mineral
7-075	Irregularity
7-079	Not Found
7-081b	Other Mineral
7-082	Other Mineral
7-098	Other Mineral
7-098	Other Mineral

Iron Correction

(a) Plot relating the SIMS $\delta^{18}O$ bias (‰) to the cation composition of the dolomite–ankerite solid solution series [Fe# = Fe/(Mg+Fe)] for a typical calibration using a 10µm diameter spot size. The sample matrix effect can be accurately estimated using the Hill equation, which is commonly employed to describe relations of 'concentration' versus 'measured effect' type, especially in systems that behave non-linearly and reach saturation. (b) Plot of the calibration residual. For most reference materials in the suite, the averaged measured value of $\delta^{18}O$ bias*(RMUW6220) differs by < 0.3‰ from the value predicted by the calibration (depicted by solid lines). Modified from Sliwinski et al., (2015). Figure from Orland et al., pers. com. (2015).

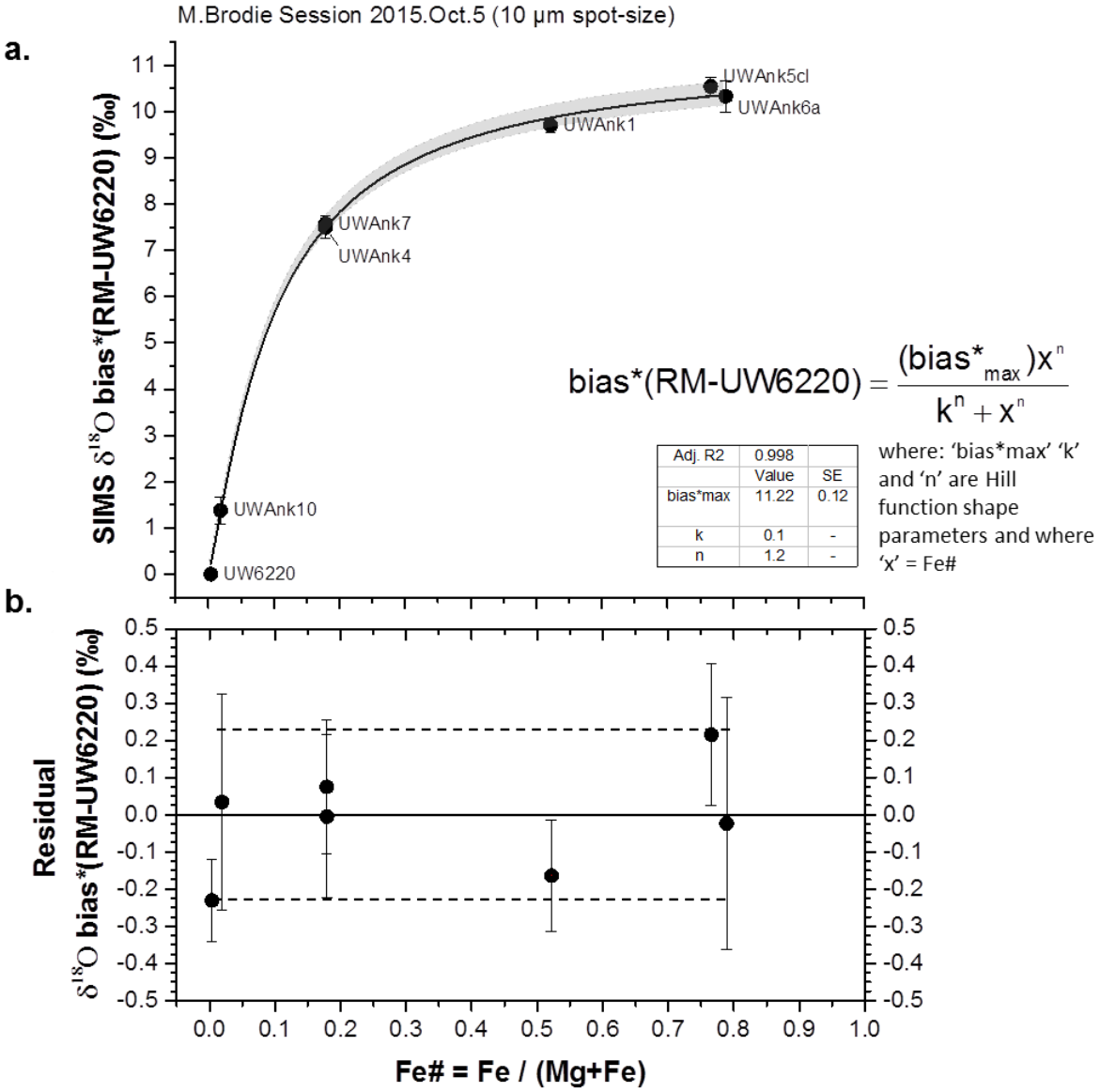
a.
M.Brodie Session 2015.Oct.5 (10 µm spot-size)
SIMS δ18O bias*(RM-UW6220) (‰)
UWAnk5cl
UWAnk6a
UWAnk1
UWAnk7
UWAnk4
UWAnk10
UW6220
bias*(RM-UW6220) = (bias*max)x^n / (k^n + x^n)
Adj. R2 0.998
Value SE
bias*max 11.22 0.12
k 0.1 -
n 1.2 -
where: 'bias*max' 'k' and 'n' are Hill function shape parameters and where 'x' = Fe#
b.
Residual
δ18O bias*(RM-UW6220) (‰)
Fe# = Fe / (Mg+Fe)

1026